Geological Survey of Norway
N-7491 Trondheim, Norway

REPORT

Report no.: 2003.105	ISSN 0800-3416	Grading: Open

Title:

Evaluation of the use of PSInSAR for the monitoring of subsidence in Oslo region

Authors:

Dehls, J. F., Nordgulen, Ø.

Client:

Oslo kommune (Friluftsetaten, Havnevesenet, Vann- og avløpsetaten, Plan- og bygningsetaten), Jernbaneverket (Region Øst)

County: Oslo

Municipality: Oslo

Map-sheet name (M=1:250.000)

Oslo

Map-sheet no. and -name (M=1:50.000)

1814 I Asker, 1914 IV Oslo

Deposit name and grid-reference:

Number of pages: 45 Price (NOK): 535

Map enclosures: 4

Fieldwork carried out:	Date of report:	Project no.:	Person responsible:
	06.02.2004	3018.01	Jan S. Rønning

Summary:

Timely identification of subsidence is important in order to ensure that remediation efforts are successful. Even if subsidence cannot be prevented or stopped, it must be accounted for in new construction planning. Identification and monitoring of ground deformation can be accomplished using a number of surveying techniques. Levelling and GPS are both expensive and the number of benchmarks that can be controlled is limited.

Since the early 1990's satellite-based radar interferometry has been used to identify large ground movements due to earthquakes and volcanic activity. Data stacking methods that take advantage of a growing archive of radar images, as well as increasing computing power, have led to a large increase in the precision of the technique. Both linear trends and seasonal fluctuations can be identified using the Permanent Scatterers technique.

The Geological Survey of Norway has been experimenting with the use of radar interferometry to detect fault movements and landslides, as well as subsidence. Recently, we have tested the feasibility of using the technique to monitor subsidence due to underground construction. The well-known subsidence caused by groundwater drainage during the construction of the Romeriksporten tunnel presents a perfect test case. In addition, subsidence in Oslo centre was examined to better understand the processes involved and possibly establish a basis for future monitoring. Subsidence due to the tunnelling activity was identified successfully in numerous buildings. Displacement-time series obtained by radar interferometry are in close agreement with those obtained by traditional surveying techniques. The onset of subsidence from west to east is in close agreement with the rate of tunnel construction.

The city of Oslo's network of benchmarks was first levelled in 1927. This network can be used to measure large-scale subsidence phenomena and serves as a reference for more local surveys. It is not dense enough, however, to identify local subsidence patterns. Nor is it measured frequently enough, to monitor this type of hazard. The pattern of subsidence identified using radar interferometry is in close agreement with the most recent subsidence determinations from the benchmark network. However, the interferometric data provide a much higher resolution dataset that can be used to study correlations with other datasets such as depth-to-basement.

Keywords:	subsidence	interferometry
urban geology		

CONTENTS

1. Introduction 1

2. Differential SAR Interferometry (DInSAR) 2

2.1 Permanent Scatterers Technique (PSInSAR) 3

2.1.1 Standard Processing vs. Advanced Processing 4

2.1.2 Notes about velocity values 4

3. Results 5

3.1 Standard processing 5

3.2 Advanced processing 6

3.3 Comparison with benchmarks 9

3.4 Comparison with depth to bedrock 15

3.5 Comparison with levelling 17

3.6 Selected examples of displacement time series 22

3.6.1 Alnabru area 22

3.6.2 Bjørvika 25

3.6.3 Stenersgata 22 26

3.6.4 Lilletorget 1 27

3.6.5 Grev Wedels plass 1 28

3.6.6 Rådhusplassen 1 29

3.6.7 Filipstad 30

3.6.8 Kongshavn kai/Sjursøya 33

3.6.9 Tøyen 34

3.6.10 Sofienberg 35

3.6.11 Ullevål 36

3.6.12 Majorstua 37

3.6.13 Colosseum Kino 38

3.6.14 Bislett stadion 39

3.6.15 Frogner stadion 40

3.6.16 Jordal Amfi 41

3.6.17 Valle Hovin stadion 42

4. Future Monitoring Possibilities 43

5. Conclusions 44

6. References 45

FIGURES

Figure 1. SAR image showing Ranafjorden and Svartisen glacier, July, 1995. 2

Figure 2. SAR interferograms obtained from a pair of images acquired July 15 and 16, 1995. The area is the same as Figure 1. Fringes are related to topography. 3

Figure 3. Displacement-time series for selected houses along the trace of the Romeriksporten tunnel. Accelerated subsidence in Hellerud and Godlia coincides with the time of tunnel construction in those areas. The subsidence in Ellingsrud shows no acceleration. 6

Figure 4. There is a very low density of PS (circles) in the region with the highest number of affected buildings (in red). In many cases, such as Hellerudveien 42B (circled in blue, see Figure 5) the rate of subsidence was too great for the method to work. 7

Figure 5. Measurements of subsidence in Hellerudveien 42B (circled in blue in Figure 4) obtained by levelling. The high rate of subsidence, combined with the tilting (bolts are on various corners of the building) made it impossible to identify any PS. 8

Figure 6. Comparison of benchmarks with nearest Permanent Scatterers. Subsidence rate for benchmarks is calculated over the last measured period. The blue arrows indicate the positions of the benchmarks in Figures 7 to 10. 10

Figure 7. Displacement-time series for C.J. Hambros plass 7 compared with historical subsidence measurements. 11

Figure 8. Displacement-time series for Frognerveien 47 compared with historical subsidence measurements. 12

Figure 9. Displacement-time series for Schweigaards Gate 15 compared with historical subsidence measurements. 13

Figure 10. Displacement-time series for benchmark on Rådhusbrygge compared with historical subsidence measurements. 14

Figure 11. Subsidence contours derived from PS analysis overlain upon depth-to-basement image. There is a good general agreement between subsidence rates and the thickness of surficial deposits. 15

Figure 12. Subsidence contours derived from PS analysis overlain upon depth-to-basement image in the Majorstua area. No significant subsidence is evident in areas with shallow surficial deposits. 16

Figure 13. Subsidence measured in Låveveien 32B (centre of photo) by levelling compared with PS from Låveveien 32, next door (PS AI479, AB282). PS velocity is along the line of sight with the satellite (23º from vertical). The yellow symbols indicate buildings that were monitored using levelling. 17

Figure 14. Subsidence measured in Stordamveien 54 by levelling compared with three of many PS from the same building. PS measurements reveal subsidence not detected by levelling, which began only afterwards. 18

Figure 15. Both levelling and PS reveal between 1 and 2 cm subsidence at Munkebekken 110-112. 19

Figure 16. Levelling at both Munkebekken 63 and Munkebekken 101 shows a steady rate of subsidence from 1997. PS analysis from Munkebekken 101 (PS AW625) shows that this subsidence has had a nearly constant rate since 1992 and cannot be related to the tunnelling activity. 20

Figure 17. One PS (PS AG474) at the north end of Hellerudveien 42A, between bolts 1 and 2, is insufficient to reveal almost 8 cm of tilting that occurred from 1996 to 1997. 21

Figure 18. Displacement-time series from south end of Verkseier Furulunds vei 49 (outlined in blue). 23

Figure 19. Displacement-time series from east end of Ole Deviks vei 32. 24

Figure 20. Almost all the data points with relative subsidence rates of 6 mm/yr or more lie within the Bjørvika/Grønland area. Within Bjørvika, subsidence rates are as high as 13 mm/yr. Displacement-time series shown is from Nylandsveien 28 (blue arrow). 25

Figure 21. Displacement-time series from Stenersgata 22 (centre of photo). 26

Figure 22. Displacement-time series from Lilletorget 1 (centre of photo). 27

Figure 23. Displacement-time series from Grev Wedels plass 1 (centre of photo). 28

Figure 24. Displacement-time series from Rådhusplassen 1 (blue arrow). 29

Figure 25. Subsidence pattern in Filipstad. Displacement-time series are shown in Figures 26 (blue arrow) and 27 (green arrow). 30

Figure 26. Displacement-time series from the gas station in Filipstad (see Figure 25 for location). 31

Figure 27. Displacement-time series from one of the warehouses in Filipstad (see Figure 25 for location). 32

Figure 28. Displacement-time series from the northernmost building in Sjursøya..... 33

Figure 29. Displacement-time series from Eiriks Gata 17 (blue arrow). 34

Figure 30. Displacement-time series from Toftes Gate 69 (blue arrow). 35

Figure 31. Displacement-time series from western corner of Ullevål hospital (blue arrow). 36

Figure 32. Displacement-time series from Kirkeveien 44 (blue arrow). 37

Figure 33. Displacement-time series from Fridtjof Nansensvei 8 (centre of photo)..... 38

Figure 34. The area around Bislett stadium is subsiding between 1.5 and 2.0 mm/yr. Two PS have subsidence rate of 5 mm/yr, however these are located on the corner of a structure supported by a wooden post. It is most likely that this post is slowly deteriorating, leading to a slow collapse of the roof. 39

Figure 35. Only three PS were identified on Frogner stadion. According to the depth to bedrock map supplied by Oslo municipality, the stadium appears to be located on shallow sediments, with the exception of the northwestern and eastern corners. One of the PS identified is shows no subsidence. The other two are located on a structure on the northwestern corner of the stadium, and show subsidence rates of 3.5 to 4 mm/yr. No field checking has been carried out to determine if this represents true subsidence or slow collapse of the structure in question..... 40

Figure 36. There is no evidence of subsidence in the area around Jordal Amfi. 41

Figure 37. Only one point on Valle Hovin stadium shows any signs of subsidence (2 mm/yr). No visual inspection has been done. 42

1. INTRODUCTION

Land subsidence is a gradual settling or sudden sinking of the Earth's surface owing to subsurface movement of earth materials. Subsidence can be caused by aquifer-system compaction, drainage of organic soils, underground mining, hydrocompaction, natural compaction, dissolution, and thawing permafrost. A recent study in the UK has estimated damages due to subsidence at £300 million (Rosenbaum and Culshaw, 2003). Although Norway is not subject to all the same types of hazards (e.g. mining, karst), there are significant areas subject to subsidence due to compaction and organic decay. Unstable marine clays are also found in many areas of Norway. In addition, anthropogenic causes of subsidence, principally ground-water extraction, intentional or unintentional, are a significant hazard. Natural or anthropogenic subsidence is a geohazard that can be identified, monitored, and in some cases, remediated.

Timely identification of subsidence is important in order to ensure that remediation efforts are successful. Even if subsidence cannot be prevented or stopped, it must be accounted for in new construction planning. Identification and monitoring of ground deformation can be accomplished using a number of surveying techniques. Levelling and GPS are the most common. Both are expensive and the number of benchmarks that can be controlled is limited. The municipality of Oslo maintains a network of levelling benchmarks. Some of these benchmarks were first levelled in 1927. This network can be used to measure large-scale subsidence phenomena and serves as a reference for more local surveys. It is not dense enough, however, to identify local subsidence patterns. Nor is it measured frequently enough, to monitor this type of hazard.

Since the early 1990's satellite-based radar interferometry has been used to identify large ground movements due to earthquakes and volcanic activity. Data stacking methods that take advantage of a growing archive of radar images, as well as increasing computing power, have led to a large increase in the precision of the technique. Numerous studies of urban subsidence using radar interferometry have been published (Amelung et al., 1999; Fruneau and Sarti, 2000; Galloway et al., 1998). Both linear trends and seasonal fluctuations can be identified (Colesanti et al., 2003a; Colesanti et al., 2003b).

NGU has been experimenting with the use of radar interferometry to detect fault movements and landslides (Dehls et al., 2002). Involvement in the project "Miljø- og samfunnstjenlige tunneler" led us to speculate that perhaps this technique could be useful in identifying and quantifying short-term subsidence due to underground construction. The well-known subsidence caused by groundwater drainage during the construction of the Romeriksporten tunnel presents a perfect test case. Levelling had been done on a number of buildings before, during and after construction. In addition, it was decided to examine subsidence in Oslo centre to better understand the processes involved and possibly establish a basis for future monitoring.

2. DIFFERENTIAL SAR INTERFEROMETRY (DINSAR)

Differential SAR Interferometry (DInSAR) is a technique that compares the phases of multiple radar images of an area to measure surface change. It first became well known after an image of the Landers Earthquake deformation field was published in the journal Nature in 1993 (Massonnett et al., 1993). The method has the potential to detect millimetric surface deformation along the sensor – target line-of-sight.

A radar satellite emits pulses of radar energy, which are scattered by the Earth's surface. When such a pulse of radar energy is reflected back to the satellite, two types of information are recorded. The first information recorded is the amplitude of the signal. This is the information displayed in typical SAR images (Figure 1). The amplitude is influenced by factors such as the surface material, the slope of the surface and surface moisture content.

Figure 1. SAR image showing Ranafjorden and Svartisen glacier, July, 1995.

The second information recorded is the phase of the wave. ERS satellites have a radar wavelength of 5.66 cm. The phase of the wave upon return depends primarily on the distance between the satellite and the surface. It is also affected by changes in the atmosphere, but this is a very small effect. If two images are acquired of the same area from the exact same position, any difference in phase is due to movements of the ground surface toward or away from the satellite during the time between the two images. If two images are acquired from different positions within a small period of time, the difference in phase can be used to determine the surface topography (Figure 2). Differences in phase between two images are easily viewed by combining, or interfering, the two phase-images. In the resulting image, the waves will either reinforce or cancel one another, depending upon the relative phases. The resulting image is called an interferogram and contains concentric bands of colour, or fringes, that are related to topography and/or surface deformation.

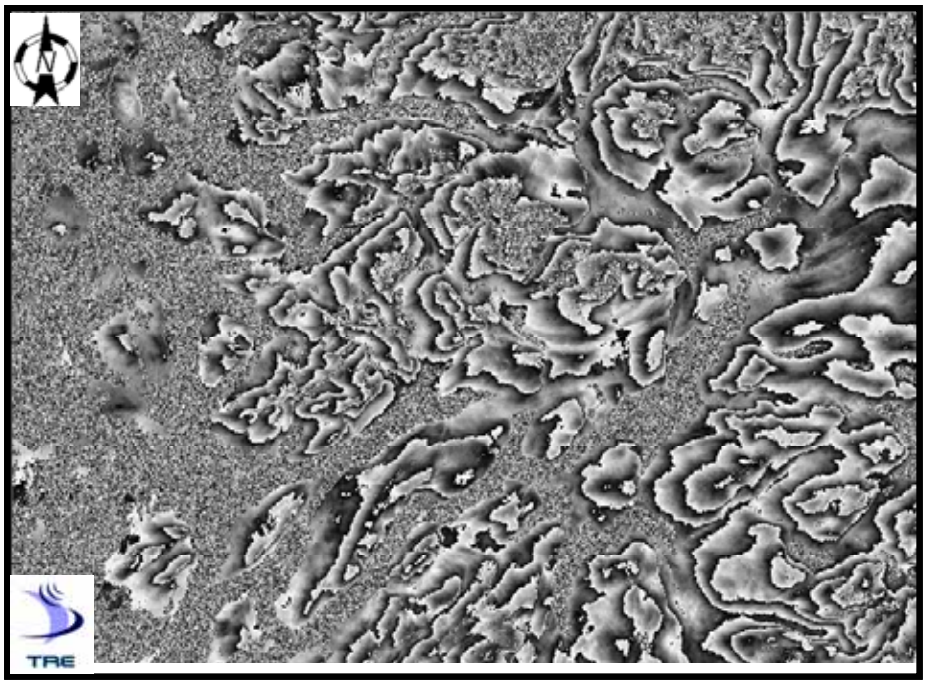

Figure 2. SAR interferograms obtained from a pair of images acquired July 15 and 16, 1995. The area is the same as Figure 1. Fringes are related to topography.

Since it is nearly impossible to obtain two images of the same area from exactly the same point at two different times, three images are typically used to analyse surface change. First, an image pair taken during a short interval is used to determine the topography. Second, an interferogram is created using two images with a longer time interval. The effects of topography are removed using the results of the first interferogram, and the resulting image contains fringes due to surface deformation. Each fringe represents one-half wavelength of surface movement. In the case of the ERS satellites, this is less than 3 cm.

Radar interferometry has one stringent condition that must be met in order for it to work. The many small reflective objects contributing to each pixel must remain unchanged, or *coherent*, between images. Decorrelation may occur due to variations in the complex reflectivity of individual sampling cells as a function of the acquisition geometry (geometric decorrelation) and/or time (temporal decorrelation). In addition, atmospheric phase screen, mainly due to the effect of the local water vapour content, can be difficult to discriminate from ground deformation.

2.1 Permanent Scatterers Technique (PSInSAR)

The SAR processing group at Politecnico di Milano has developed a new method based upon the identification of stable natural reflectors (called permanent scatterers) that are coherent over a long period of time (Ferretti et al., 2001). These permanent scatters (PS) can be identified and used in many images over a long period of time.

The PS approach is a two-step processing technique aimed at isolating the different phase terms (atmospheric phase screen, deformation and residual topography) on a sparse grid of phase stable, point-wise radar targets. The PS approach is based on the exploitation of long time-series of interferometric SAR data (at least 25-30 images). The technique is able to overcome both main limiting factors: PS are only slightly affected by decorrelation and can be used to estimate and remove the atmospheric phase screen.

The sparse PS grid can be thought of as a high spatial density (up to 400 PS/km2, in highly urbanized areas) geodetic network allowing ground deformation measurements (along the line-of-sight direction) with millimetric accuracy (0.1-1 mm/yr on the average line-of-sight deformation rate and 1-3.5 mm on single measures).

Since Permanent Scatterers mainly correspond to portions of man-made structures, and a minimum PS density is required to guarantee the measurements reliability, most significant PS results have been obtained analyzing urban areas and their immediate neighbourhood. The PS approach allows the identification of isolated phase-stable targets in low coherence areas. These provide precise surface deformation data in areas where a conventional DInSAR approach fails due to decorrelation noise.

2.1.1 Standard Processing vs. Advanced Processing

Standard PS processing is fully automatic, with quality checks performed only on the final results. A linear rate of movement is assumed and search parameters are optimized to process areas up to several thousand square kilometres. Advanced processing can be performed on smaller areas once ground motion is identified. The main differences with advanced processing are:

- finer sampling grid of the focused and fitted data.
- lower thresholds for atmospheric phase screen estimation and removal to obtain a higher PS density.
- ad hoc procedures are carried out for a better detection of seasonal motion or abrupt steps in rate of movement. No "a priori" models on the PS behaviour are imposed.
- manual control by the operator for a better refining and calibration of the processing parameters.

2.1.2 Notes about velocity values

Several points must be kept in mind when interpreting the velocity values obtained by this method.

- All values are relative to an arbitrarily chosen reference point that is assumed to be stable.
- The standard deviation of velocity errors increases with distance from the reference point. For this reason, the reference point is chosen as close as possible to the centre of the area of interest.
- As stated earlier, the velocity given is the velocity along the line-of-sight to the satellite, which is on average 23º from the vertical. If the true movement direction is vertical, the line-of-sight velocity is an underestimate of the true velocity.
- No images are available for 1994 and early 1995. During that year, the European Space Agency used the ERS-1 satellite for several different missions that had a different orbital geometry.

3. RESULTS

3.1 Standard processing

In the current project, standard processing was performed on two independent series of radar images. This was possible due to the large overlap between images from neighbouring orbits at this high latitude. 42 images from track 108 and 48 images from track 337 were processed, covering the time period 1992 to 2002. One of the gyroscopes onboard the ERS-2 satellite failed on January 7, 2001, and very few images acquired since then have been of sufficient quality to use for interferometry.

By processing two sets of images, we obtained two independent datasets that could be compared at a regional and local scale. In addition, since the acquisition geometry was slightly different, only a subset of the PS in the two dataset corresponds to the same objects. Thus we obtained a higher total density of measurements.

Maps 1 and 2 show the two velocity fields over Oslo municipality. The PS density is clearly related to the density of man-made structures. The highest density, in the city center, is over 300 PS/km^2 in track 108 and over 1200 PS/km^2 in track 337. In residential areas, such as Ullern, the PS density is approximately 100 PS/km^2 in track 108 and 350 PS/km^2 in track 337. Map 2 (track 337) shows a higher PS density, especially in the eastern part of Oslo. This is due to the difference in orbital track and acquisition geometry. Data from this track were used for further processing (see next section).

Since the two datasets were processed independently, each has its own arbitrarily chosen reference point, which is considered stable. For this reason, the velocity values vary slightly from one dataset to the other. Nonetheless, the pattern of subsidence is identical in both datasets.

3.2 Advanced processing

Advanced processing was carried out over two areas. The first area covers central Oslo, from Sjursøya in the south to Ullevål in the north. The results from this area are shown in Map 3. The PS density in the city center is 2200 PS/km^2 in the new dataset. This represents an increase of over 80% from the standard processing.

Significant subsidence is occurring in the Bjørvika/Grønland area, parts of Grünerløkka, Majorstuen, Ullevål and Bislett, and in various locations along the fjord. No significant cases of non-linear subsidence were identified, although not all possible displacement-time series were examined.

The second area covers the western part of Romeriksporten tunnel, as well as the Alnabru area to the north. The area processed includes the areas most affected by the groundwater withdrawal associated with tunnel construction. The results from this area are presented in Map 4. The most striking feature is the subsidence in the Alnabru area, probably due to compaction of surficial deposits. Within the Godlia and Hellerud areas, there is no obvious pattern of subsidence revealed by the average displacement rate.

In order to identify subsidence related to the tunnelling activity, displacement-time series were generated for all points, including those with low coherence. These charts were then examined to identify non-linear displacement. Numerous houses show onset or acceleration of subsidence during the time of tunnelling. Indeed, subsidence in Godlia clearly began before subsidence in Hellerud (Figure 3). In other cases, ongoing subsidence shows no acceleration during the time of tunnelling. These results are discussed in more detail in section 3.6.

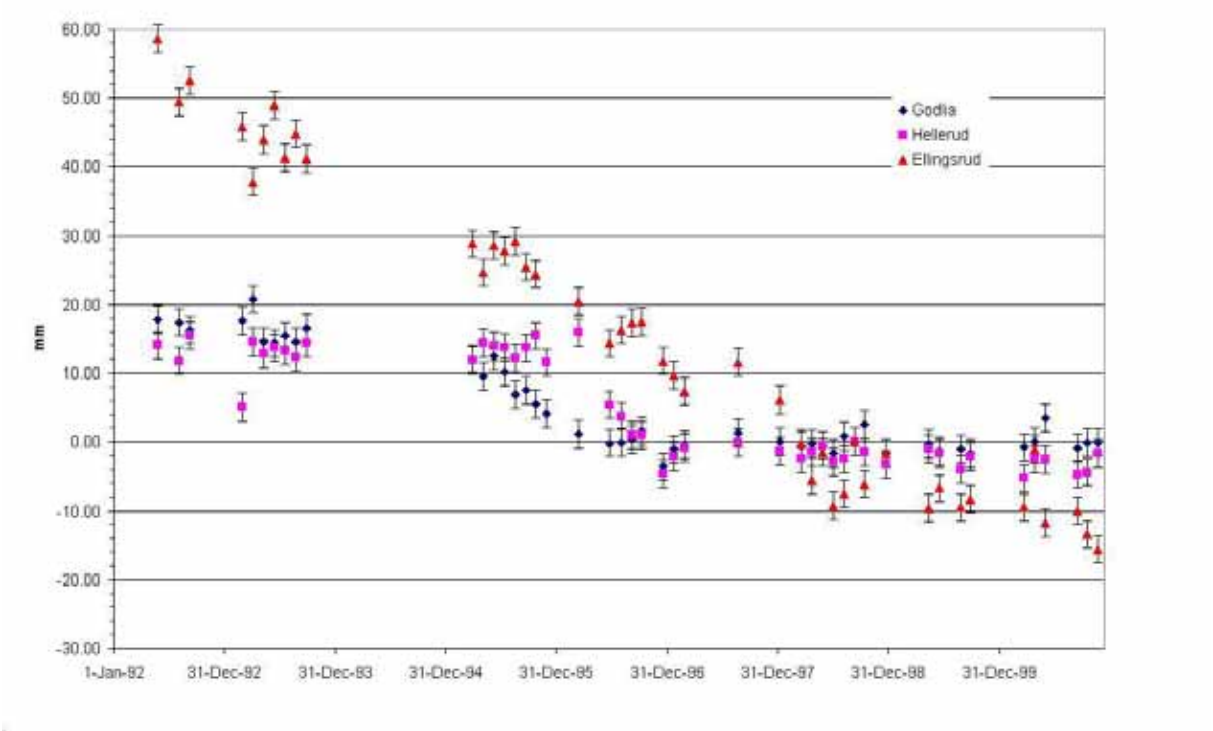

Figure 3. Displacement-time series for selected houses along the trace of the Romeriksporten tunnel. Accelerated subsidence in Hellerud and Godlia coincides with the time of tunnel construction in those areas. The subsidence in Ellingsrud shows no acceleration.

Figure 4 shows the location of houses in Hellerud where an independent study (Faggruppen for setningsskader, 2002) has confirmed subsidence and damage due to the tunnelling activities. There is a clear reduction in PS density in the area most affected. There are several possible explanations for this.

- The rate of subsidence was great enough to lead to phase unwrapping error. In other words, displacement of more than one half wavelength took place between successive image acquisitions.

- The deformation led to a change in orientation of the scattering objects, leading to decorrelation. This could be the case where houses experienced significant tilting (Figure 5).

- Reconstruction or significant repairs during the period of analysis led to a change in the surface of the building. In other words, there were no *permanent* scatterers.

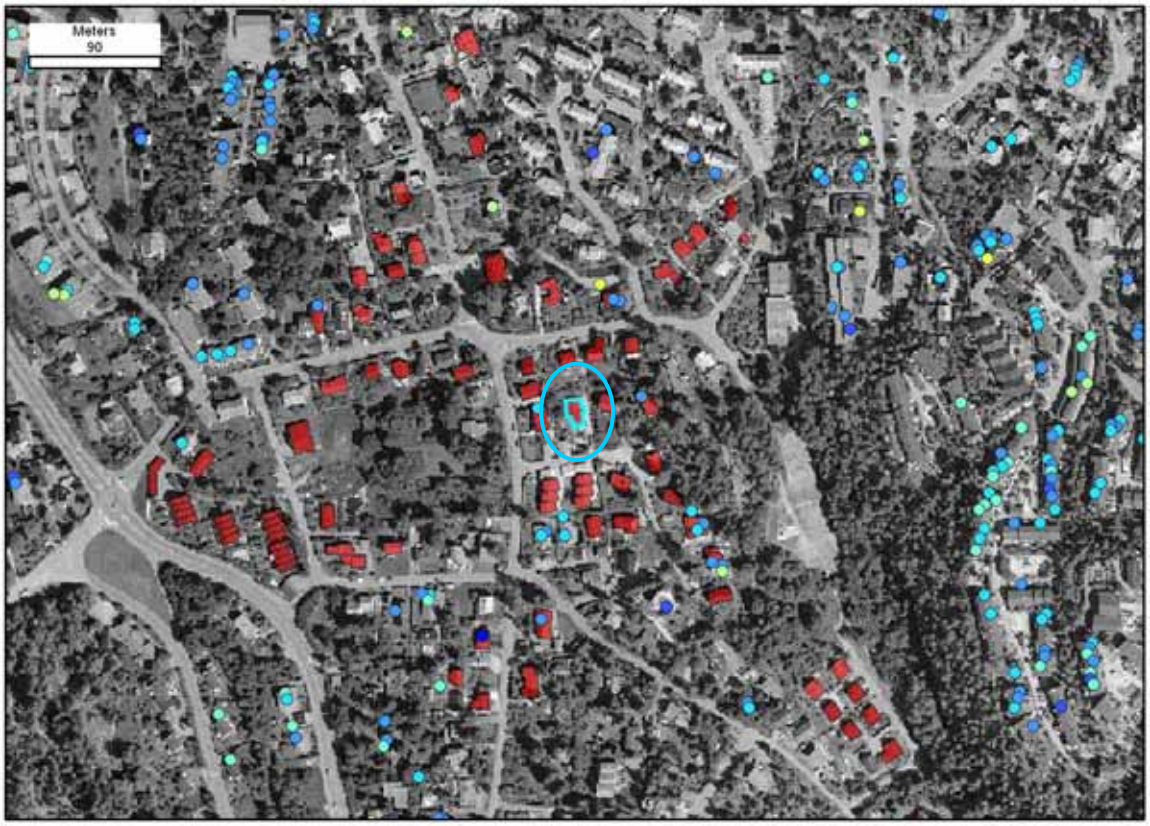

Figure 4. There is a very low density of PS (circles) in the region with the highest number of affected buildings (in red). In many cases, such as Hellerudveien 42B (circled in blue, see Figure 5) the rate of subsidence was too great for the method to work.

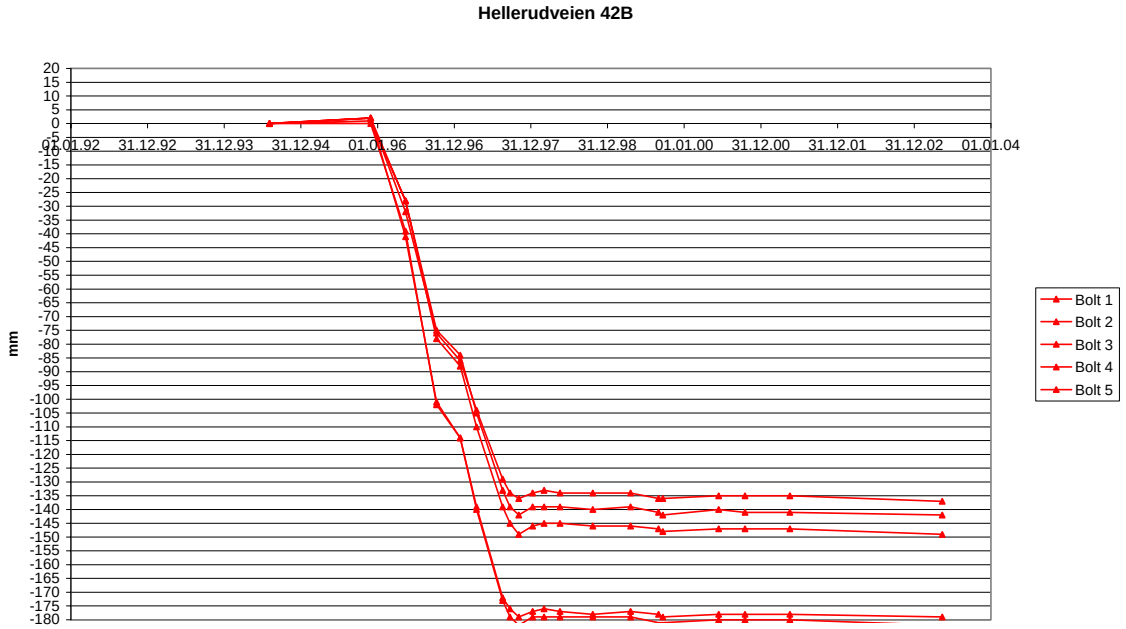

Figure 5. Measurements of subsidence in Hellerudveien 42B (circled in blue in Figure 4) obtained by levelling. The high rate of subsidence, combined with the tilting (bolts are on various corners of the building) made it impossible to identify any PS.

3.3 Comparison with benchmarks

Oslo municipality building authority (plan- og bygningsetaten) supplied the locations and recorded measurements for their grid of reference benchmarks. The earliest records are from 1927 and the most recent from 1998. Just over 500 benchmarks had been levelled more than once, allowing a calculation of subsidence rate. The rate was calculated for each benchmark for the last measured period. This period ranged from 1 to 50 years.

Figure 6 shows all the benchmarks that were within 100 metres of a PS, and all the PS that were within 100 metres of these benchmarks. The colour scale is the same for both sets of data. A general agreement is evident. However, there are some cases where the two values are quite different. Figures 7 and 8 show two examples. In both cases, the benchmark shows a marked acceleration prior to the current study, followed by a return to the historic subsidence rate.

Figures 9 and 10 show more typical examples of the remainder of the benchmarks, with the current subsidence rates matching the historic rates.

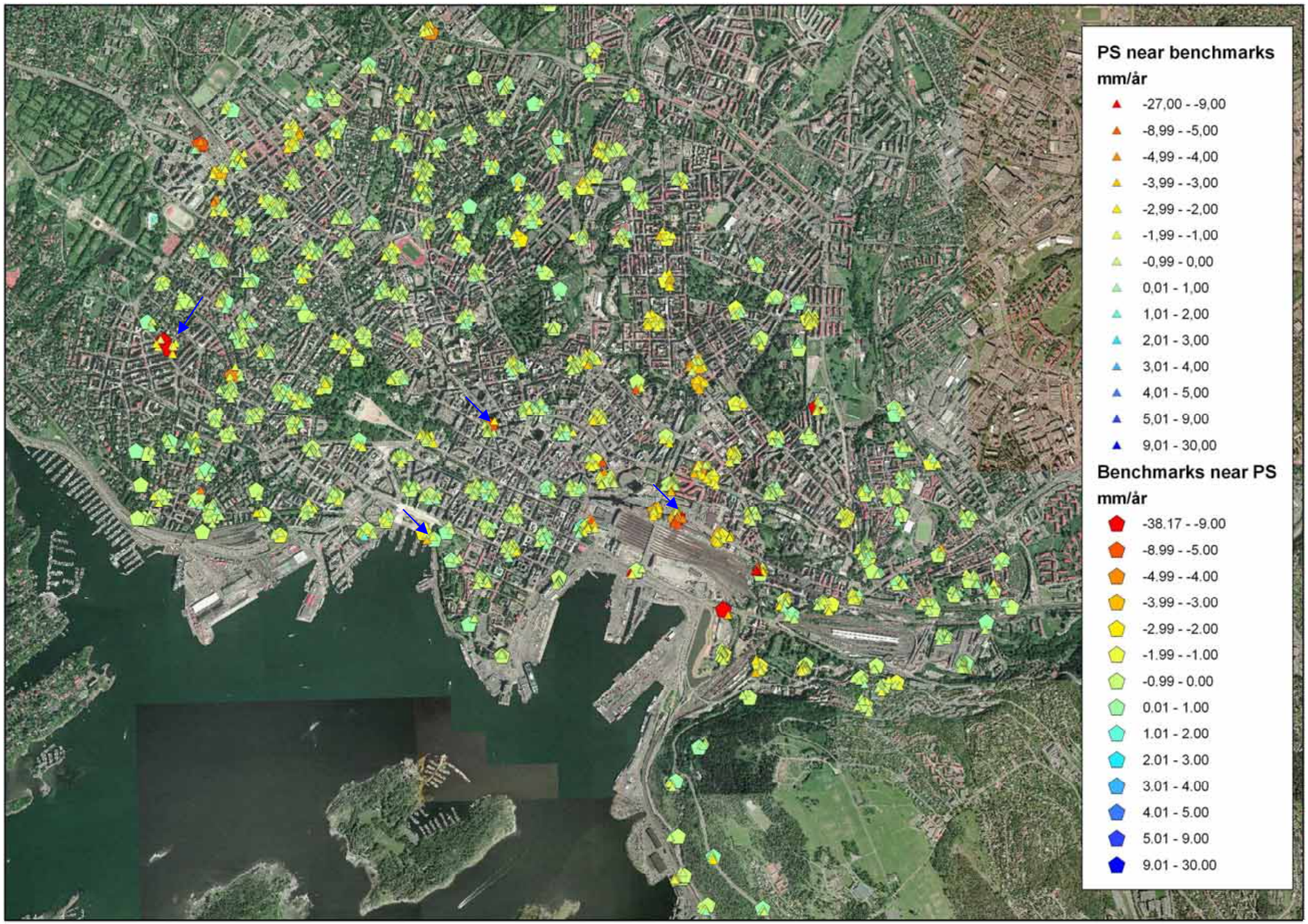

Figure 6. Comparison of benchmarks with nearest Permanent Scatterers. Subsidence rate for benchmarks is calculated over the last measured period. The blue arrows indicate the positions of the benchmarks in Figures 7 to 10.

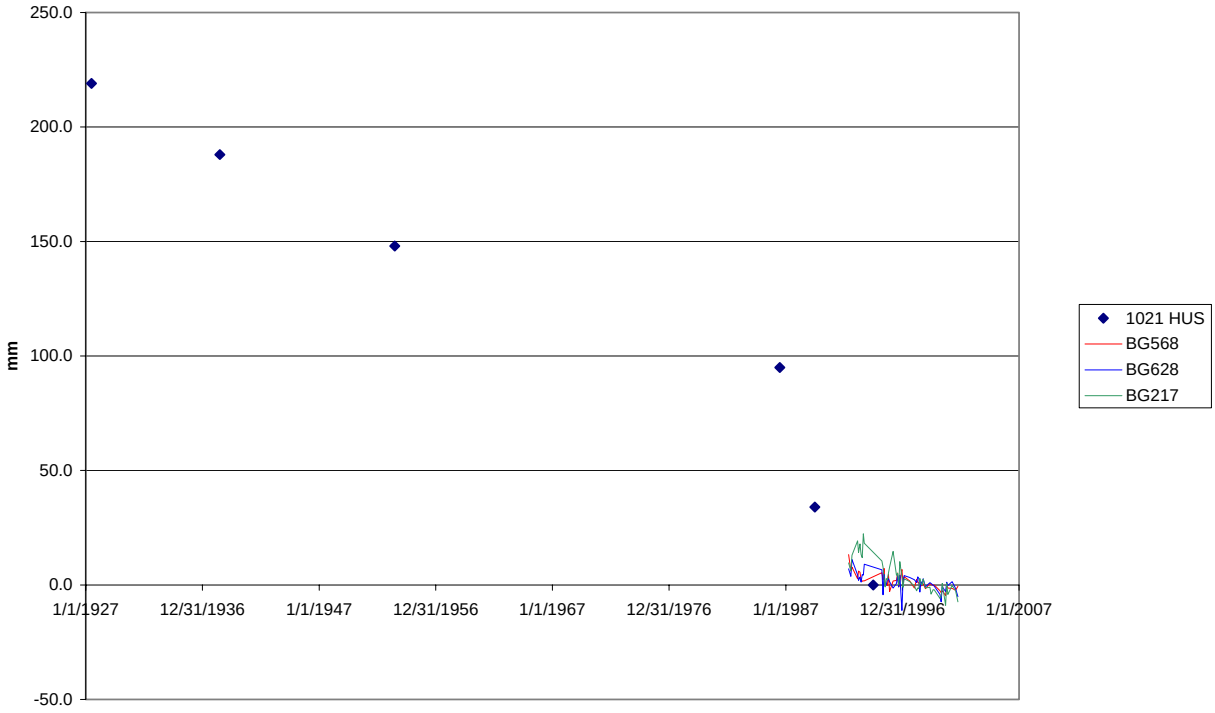

Figure 7. Displacement-time series for C.J. Hambros plass 7 compared with historical subsidence measurements.

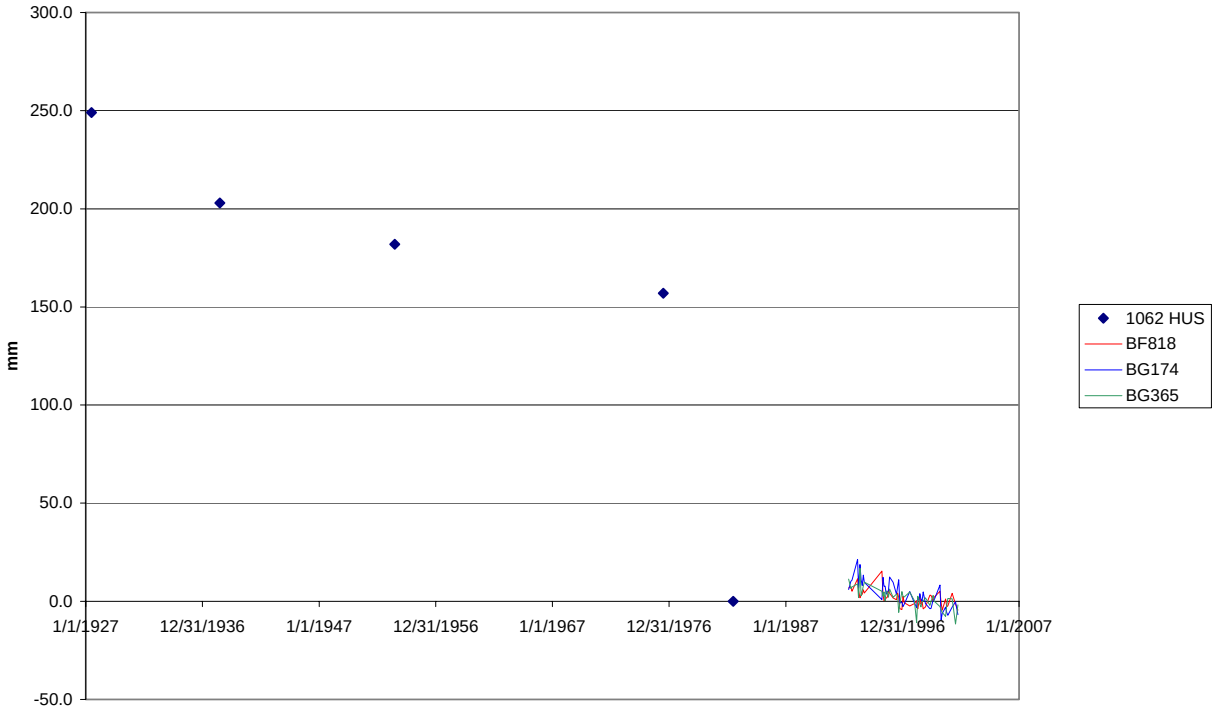

Figure 8. Displacement-time series for Frognerveien 47 compared with historical subsidence measurements.

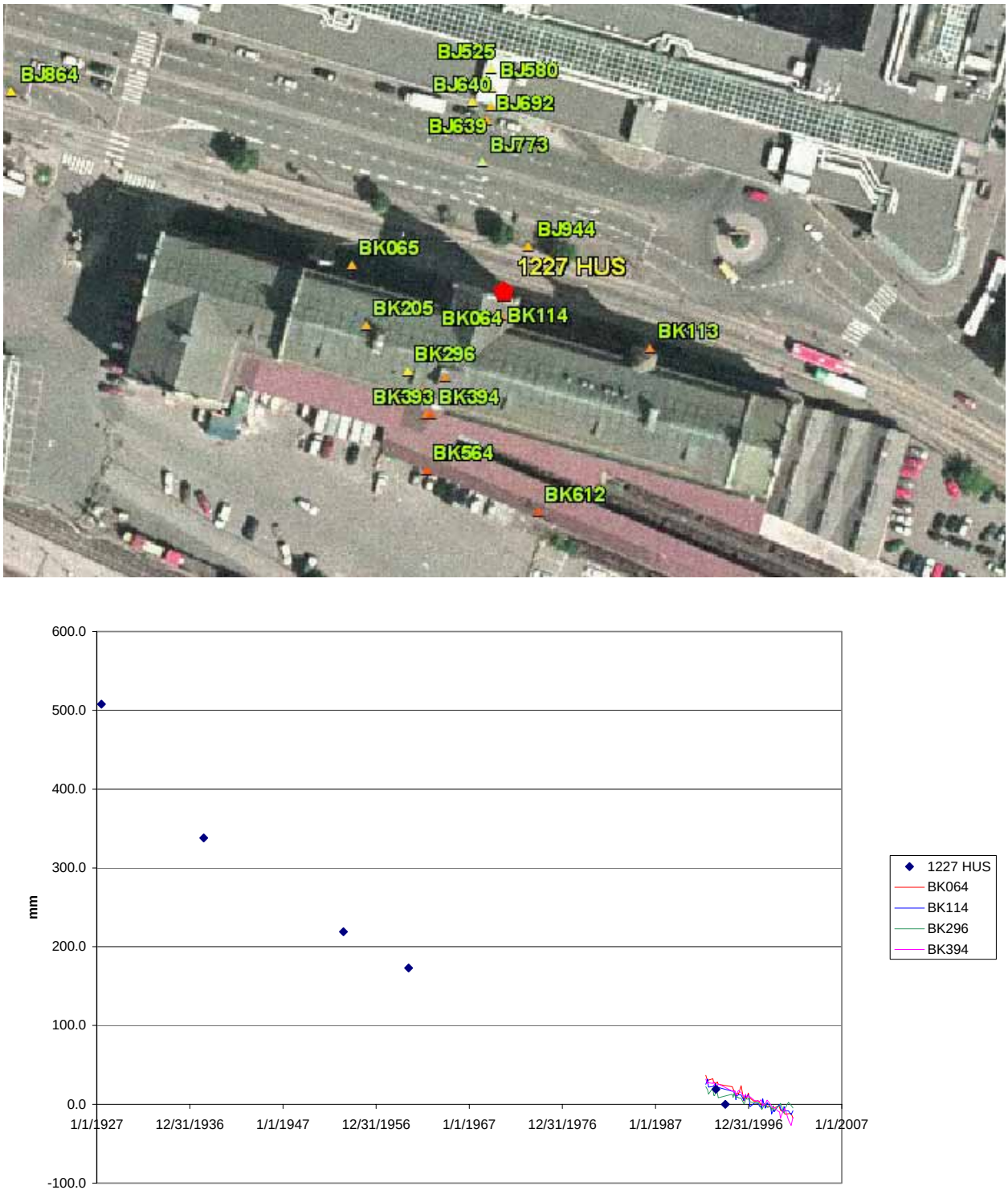

Figure 9. Displacement-time series for Schweigaards Gate 15 compared with historical subsidence measurements.

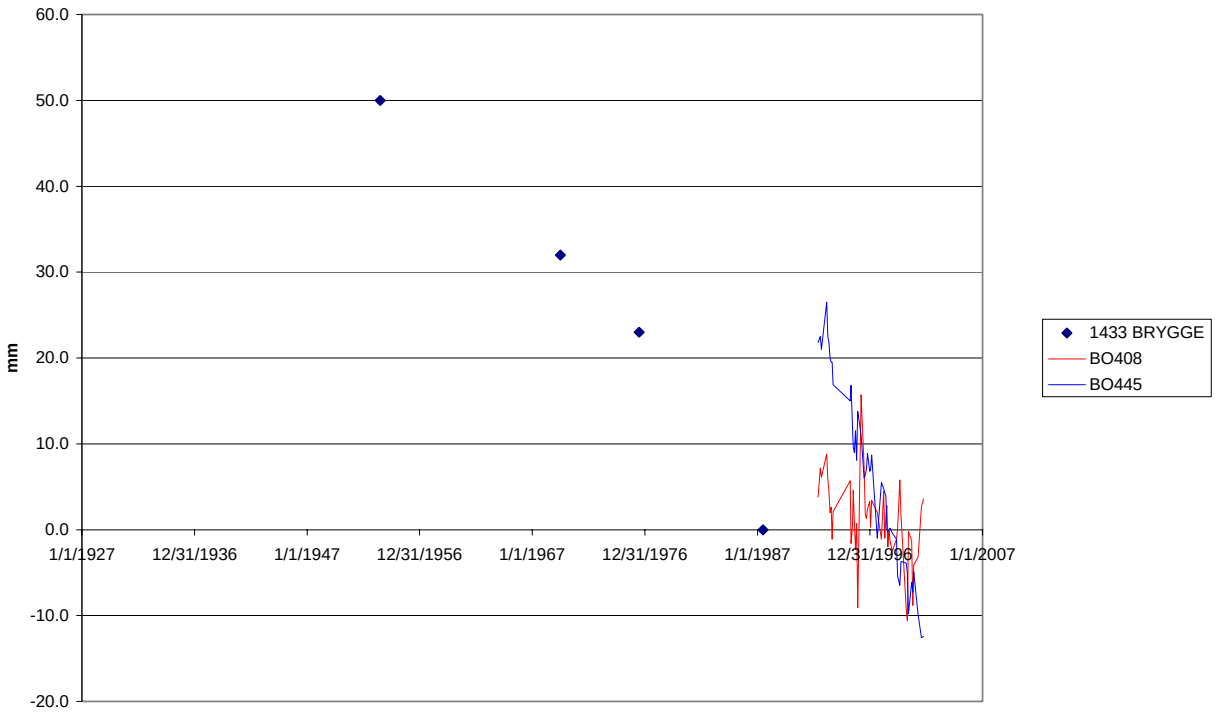

Figure 10. Displacement-time series for benchmark on Rådhusbrygge compared with historical subsidence measurements.

3.4 Comparison with depth to bedrock

Since most subsidence is caused by some type of sediment compaction, it is logical to assume that there would be a relationship between the rate of subsidence and the thickness of the sediments. A printed map showing approximate depth to bedrock was supplied by Oslo municipality. The map was scanned and georeferenced. Subsidence rates from the PS analysis for Oslo centre were interpolated onto a regular grid using an inverse distance function.

Figure 11 shows the subsidence contours overlain upon the depth-to-basement image. A general agreement is readily apparent. A closer look at Majorstua (Figure 12) confirms this pattern. A more quantitative comparison would be useful, however, that would require access to detailed depth-to-bedrock measurements in a point form. Naturally, there are other factors that influence the rate of subsidence as well, such as variations in pore-pressure, type of sediment and human activity.

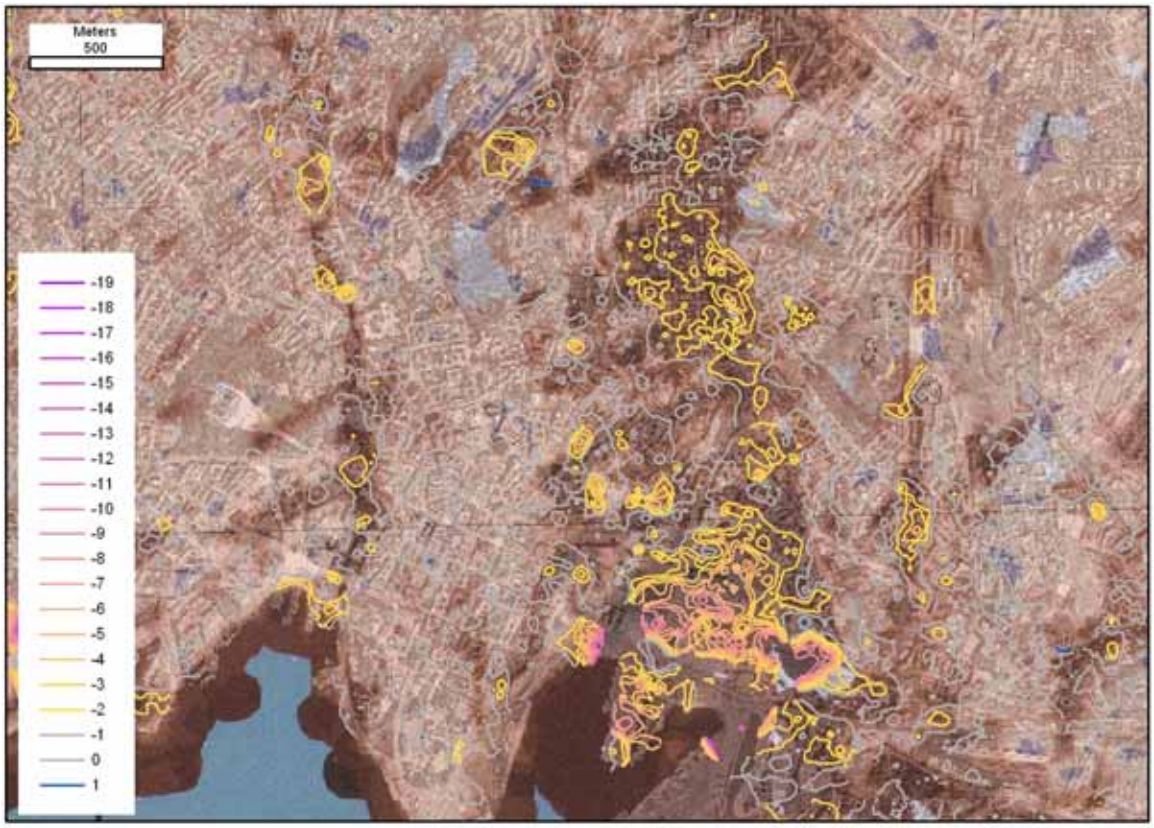

Figure 11. Subsidence contours derived from PS analysis overlain upon depth-to-basement image. There is a good general agreement between subsidence rates and the thickness of surficial deposits.

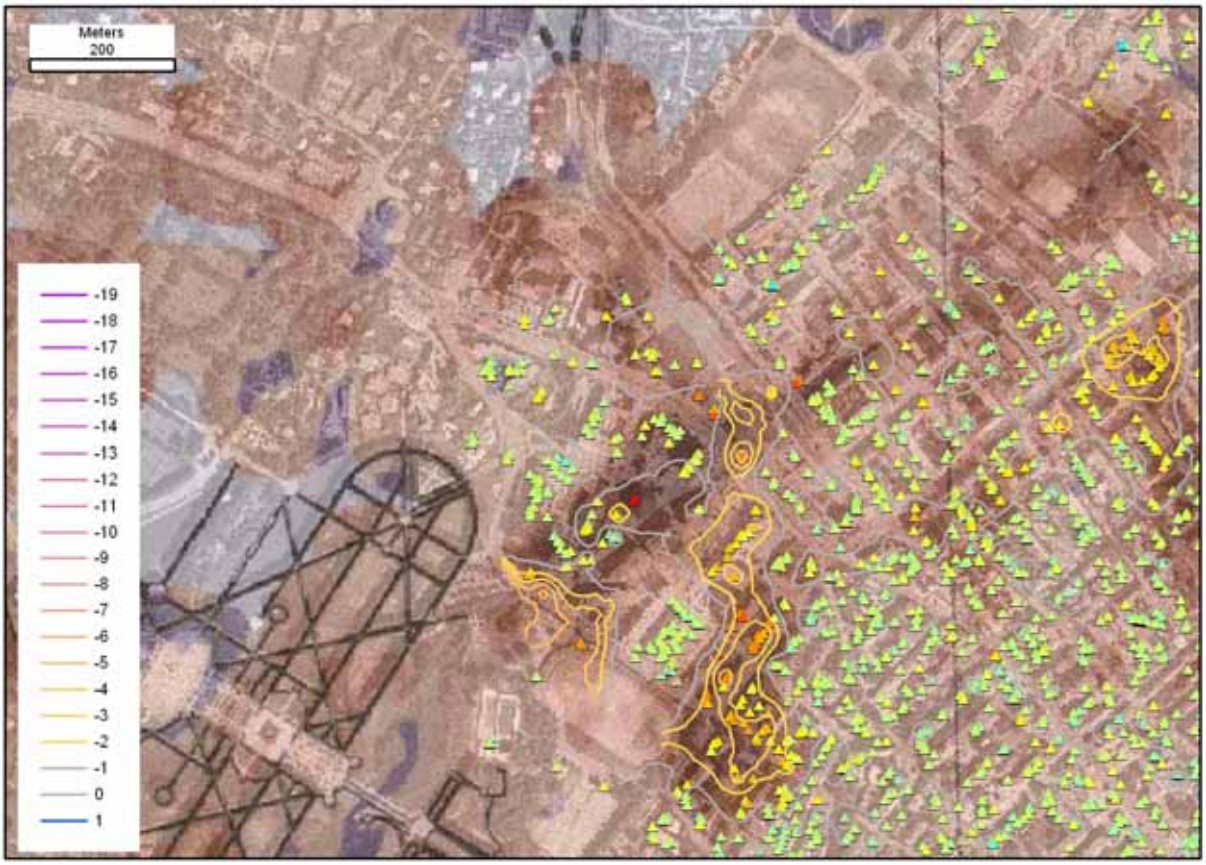

Figure 12. Subsidence contours derived from PS analysis overlain upon depth-to-basement image in the Majorstua area. No significant subsidence is evident in areas with shallow surficial deposits.

3.5 Comparison with levelling

Jernbaneverket had, and still has, a program for monitoring subsidence related to the construction of Romeriksporten tunnel. Many buildings were levelled before, during and after tunnel construction. Others were levelled only after subsidence was detected. We were supplied with the levelling data from a number of houses in Hellerud, Godlia and Ellingsrud in order to evaluate the results of the PS technique.

In the following figures, time series from permanent scatterers have been shown, even if they have low coherence. Since the signal-to-noise ratio for these points is quite low, individual displacements between successive images are cannot be measured accurately. Nonetheless, the general trends show clear offsets that compare well with independent observations.

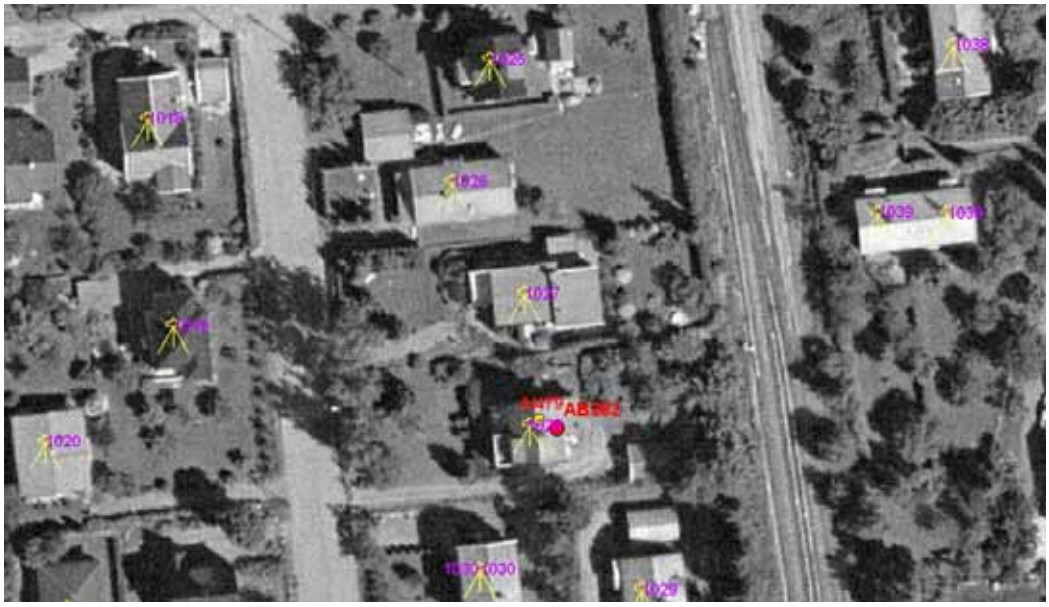

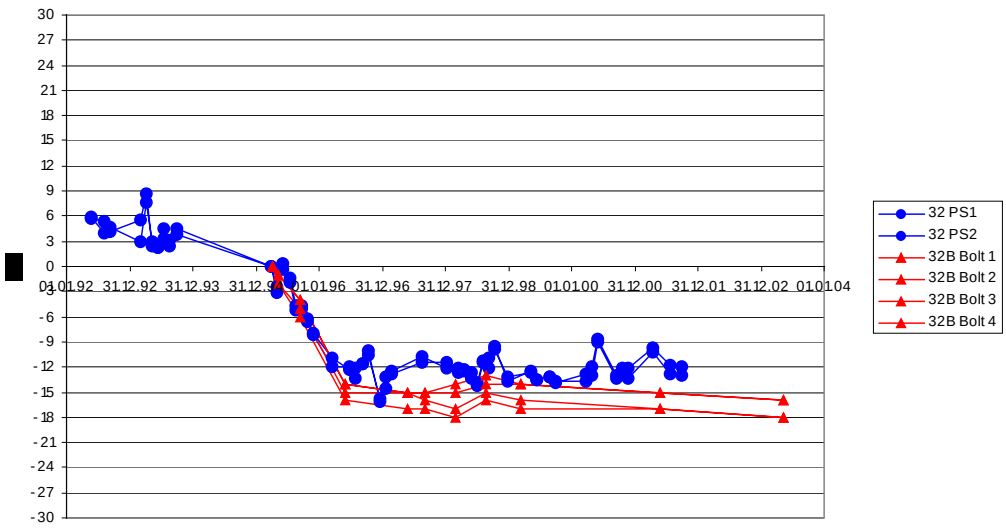

Figure 13. Subsidence measured in Låveveien 32B (centre of photo) by levelling compared with PS from Låveveien 32, next door (PS AI479, AB282). PS velocity is along the line of sight with the satellite (23º from vertical). The yellow symbols indicate buildings that were monitored using levelling.

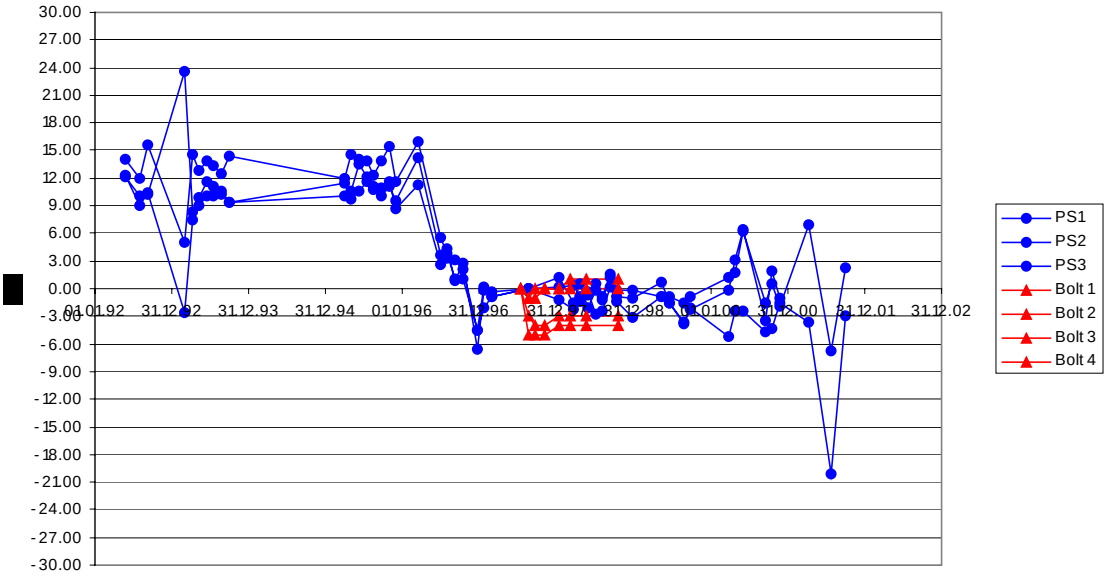

Figure 14. Subsidence measured in Stordamveien 54 by levelling compared with three of many PS from the same building. PS measurements reveal subsidence not detected by levelling, which began only afterwards.

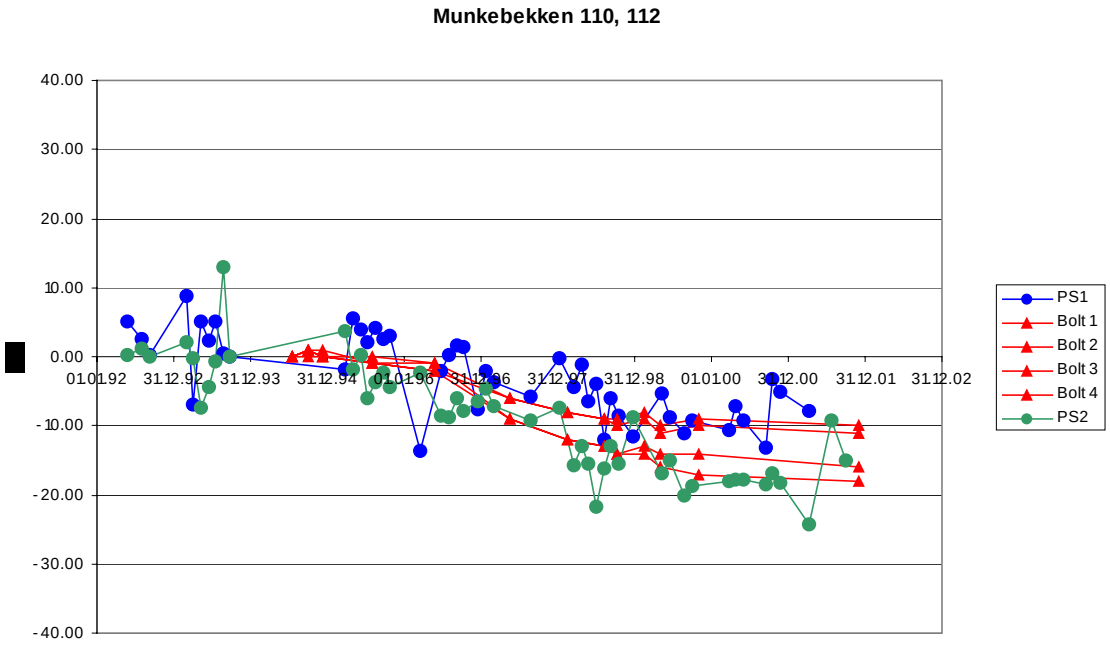

Figure 15. Both levelling and PS reveal between 1 and 2 cm subsidence at Munkebekken 110-112.

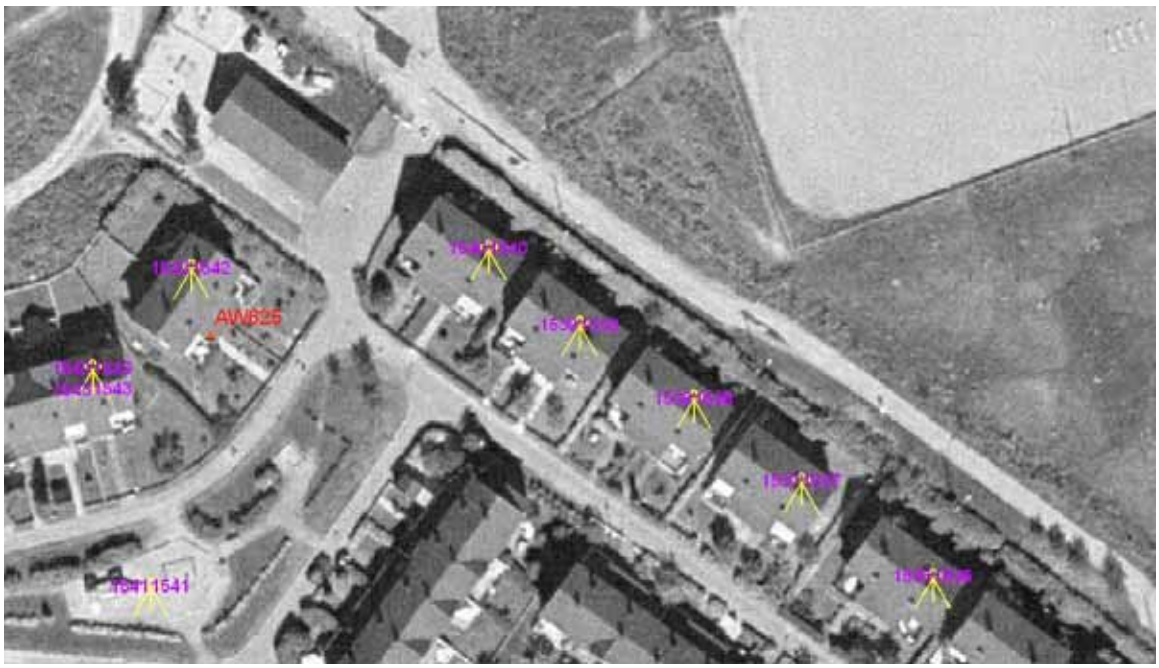

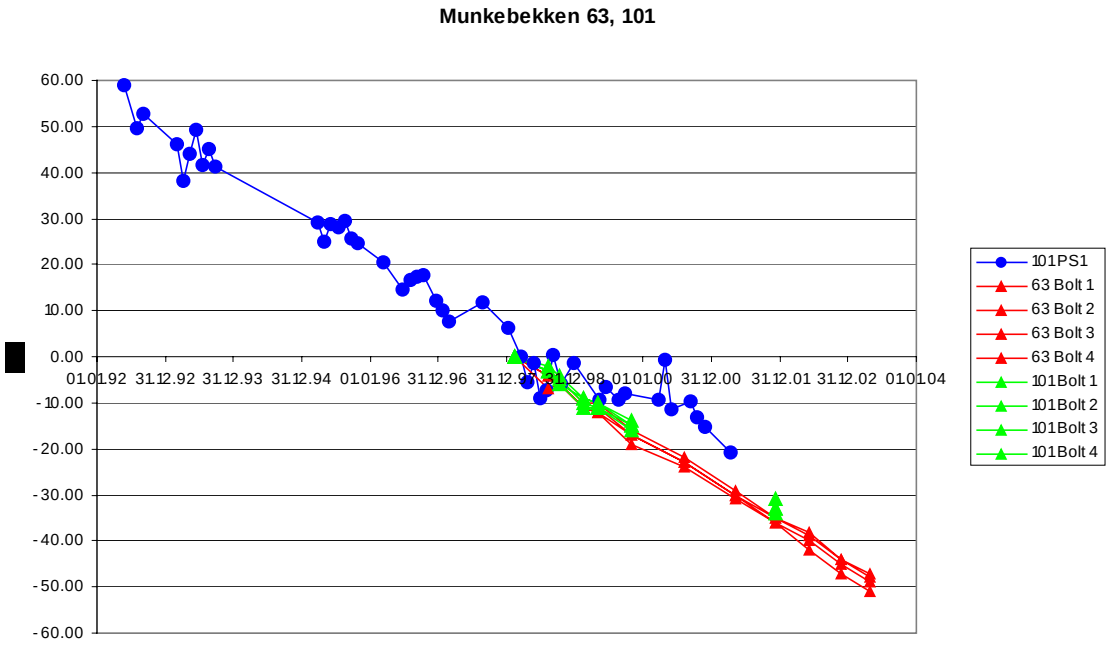

Figure 16. Levelling at both Munkebekken 63 and Munkebekken 101 shows a steady rate of subsidence from 1997. PS analysis from Munkebekken 101 (PS AW625) shows that this subsidence has had a nearly constant rate since 1992 and cannot be related to the tunnelling activity.

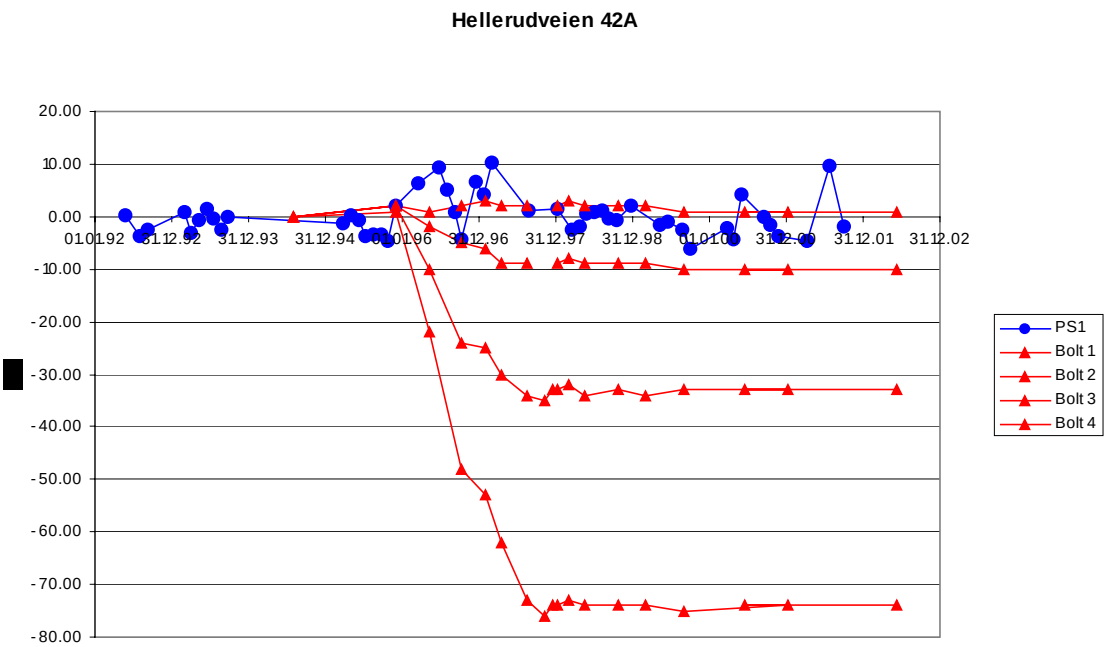

Figure 17. One PS (PS AG474) at the north end of Hellerudveien 42A, between bolts 1 and 2, is insufficient to reveal almost 8 cm of tilting that occurred from 1996 to 1997.

3.6 Selected examples of displacement time series

Based upon data obtained from advanced PS analysis, displacement-time series can be shown for individual PS. This has been done for selected areas where significant subsidence is evident. Figures 18 to 37 show displacement-time series for a few PS that are representative of the subsidence in these areas. It is possible to derive similar charts for several thousand other PS.

It should be noted that there is a varying signal-to-noise ratio throughout the dataset. This ratio is quantified by a value called the *coherence*. Although the maps and figures in this report show the velocity values for all points with coherence better than 0.65, reliable time series should only be extracted for points with coherence better than about 0.80. This threshold value is dependant upon the number of scenes processed for an area. Of the more than 20000 PS in the Oslo centre dataset, more than 7000 PS meet this criterion. Of the more than 10000 PS in the Romeriksporten area dataset, more than 3500 PS meet this criterion.

3.6.1 Alnabru area

In the northeastern end of Alnabru, north of the E6, is a former waste disposal site (Helge Sem, pers. comm.). In this area individual buildings show subsidence more than 20 mm/yr. One large building, built over the edge of the site, shows differential subsidence from one end to the other (Figure 18). Another building on Ole Deviks vei shows a similar subsidence pattern with associated structural damage (Figure 19).

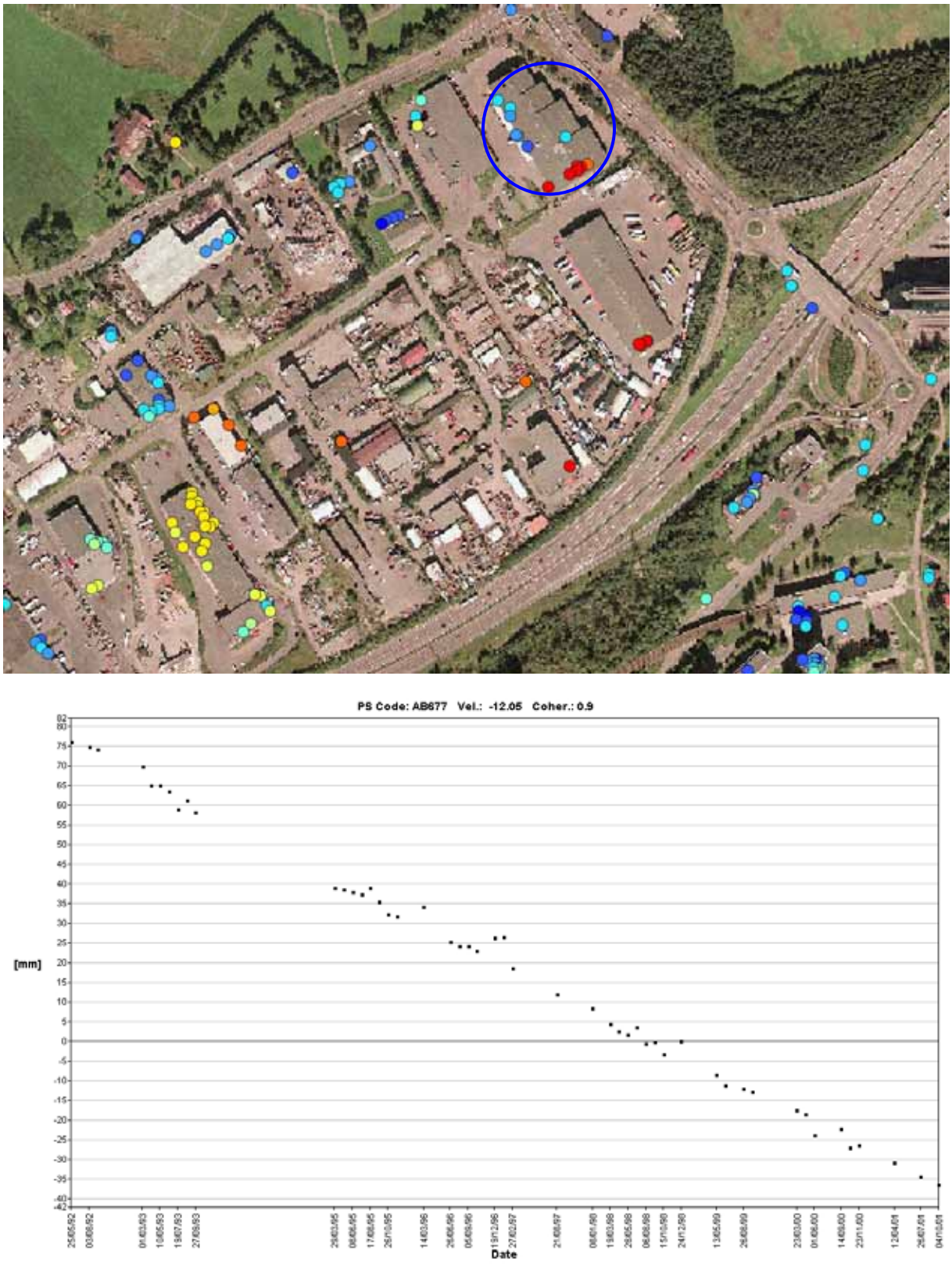

Figure 18. Displacement-time series from south end of Verkseier Furulunds vei 49 (outlined in blue).

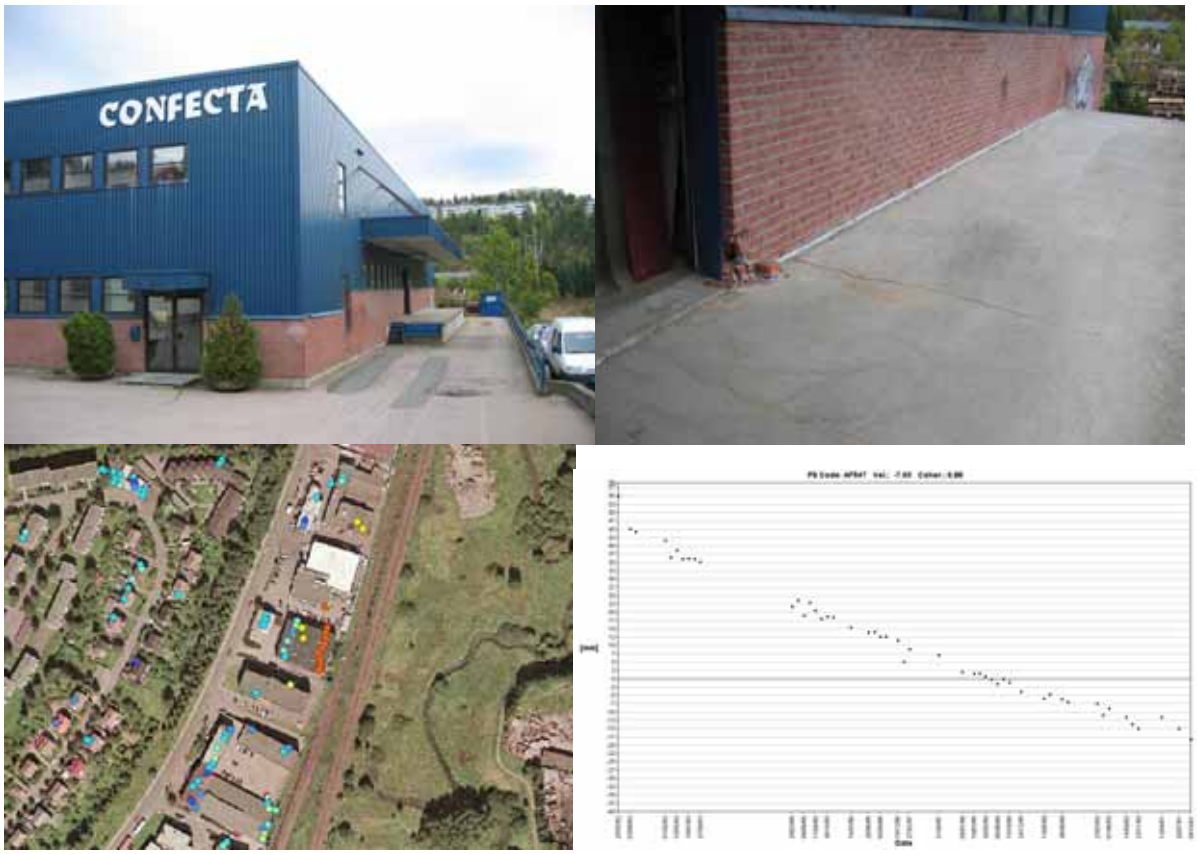

Figure 19. Displacement-time series from east end of Ole Deviks vei 32.

3.6.2 Bjørvika

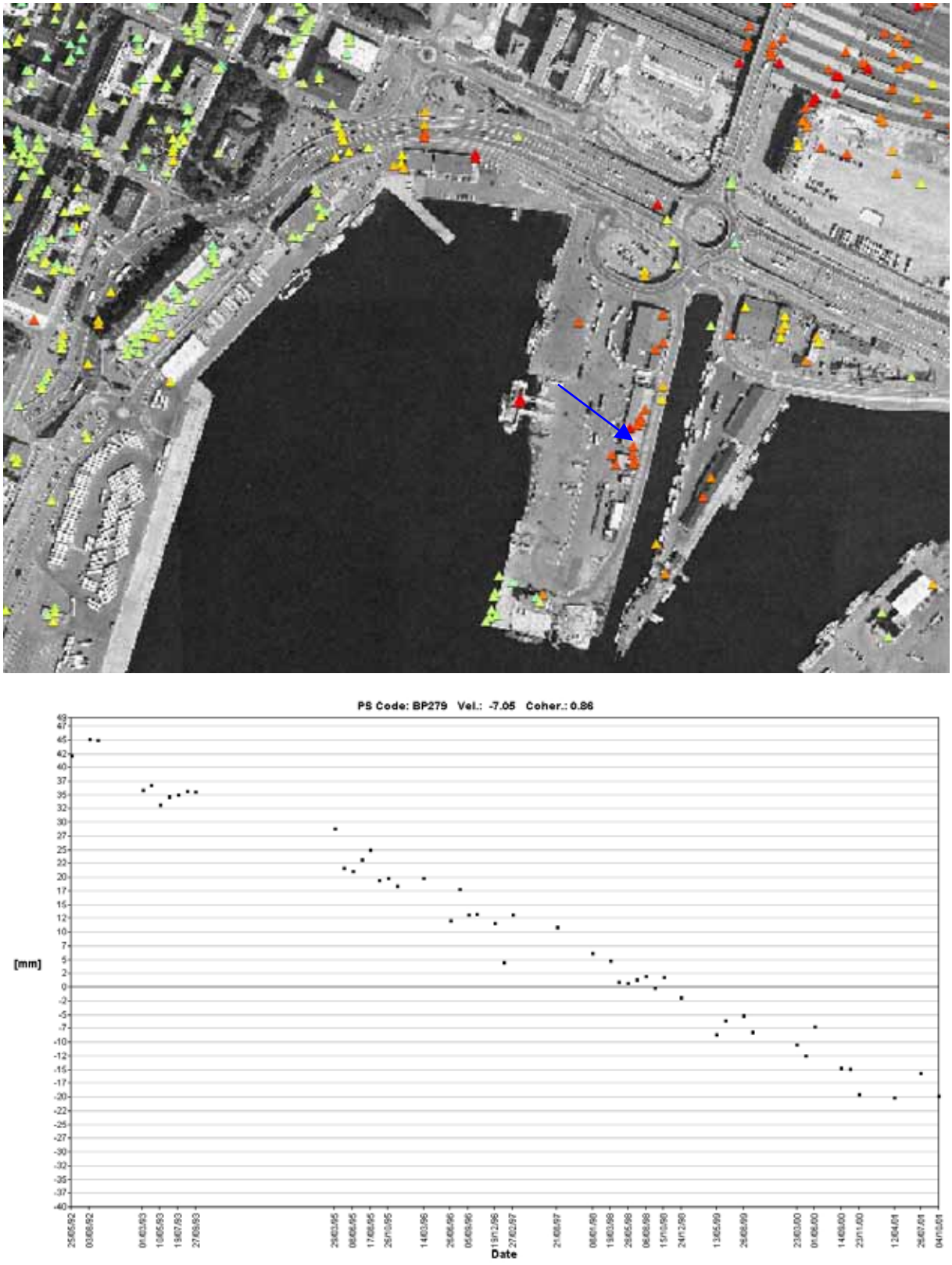

Figure 20. Almost all the data points with relative subsidence rates of 6 mm/yr or more lie within the Bjørvika/Grønland area. Within Bjørvika, subsidence rates are as high as 13 mm/yr. Displacement-time series shown is from Nylandsveien 28 (blue arrow).

3.6.3 Stenersgata 22

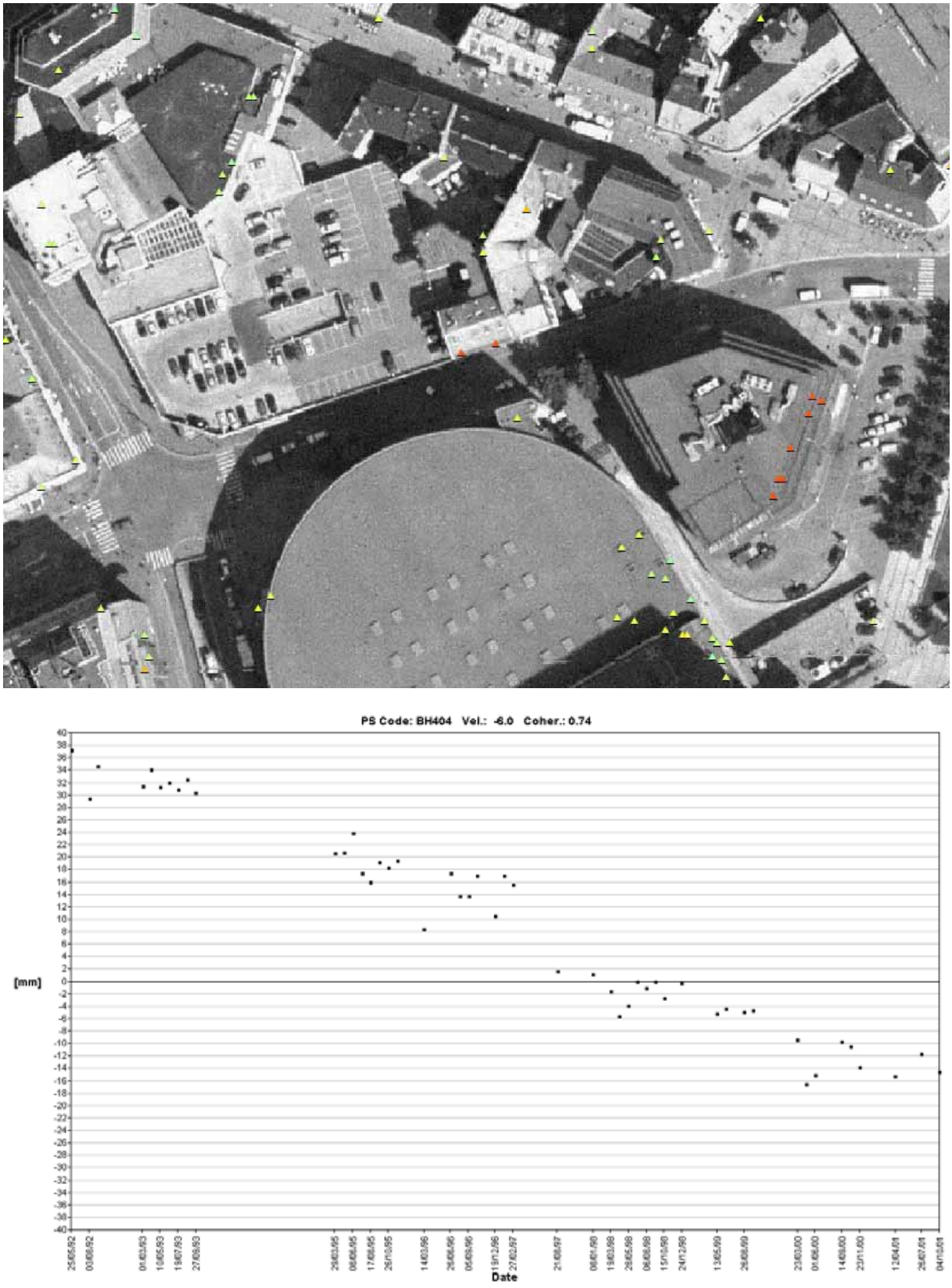

Figure 21. Displacement-time series from Stenersgata 22 (centre of photo).

3.6.4 Lilletorget 1

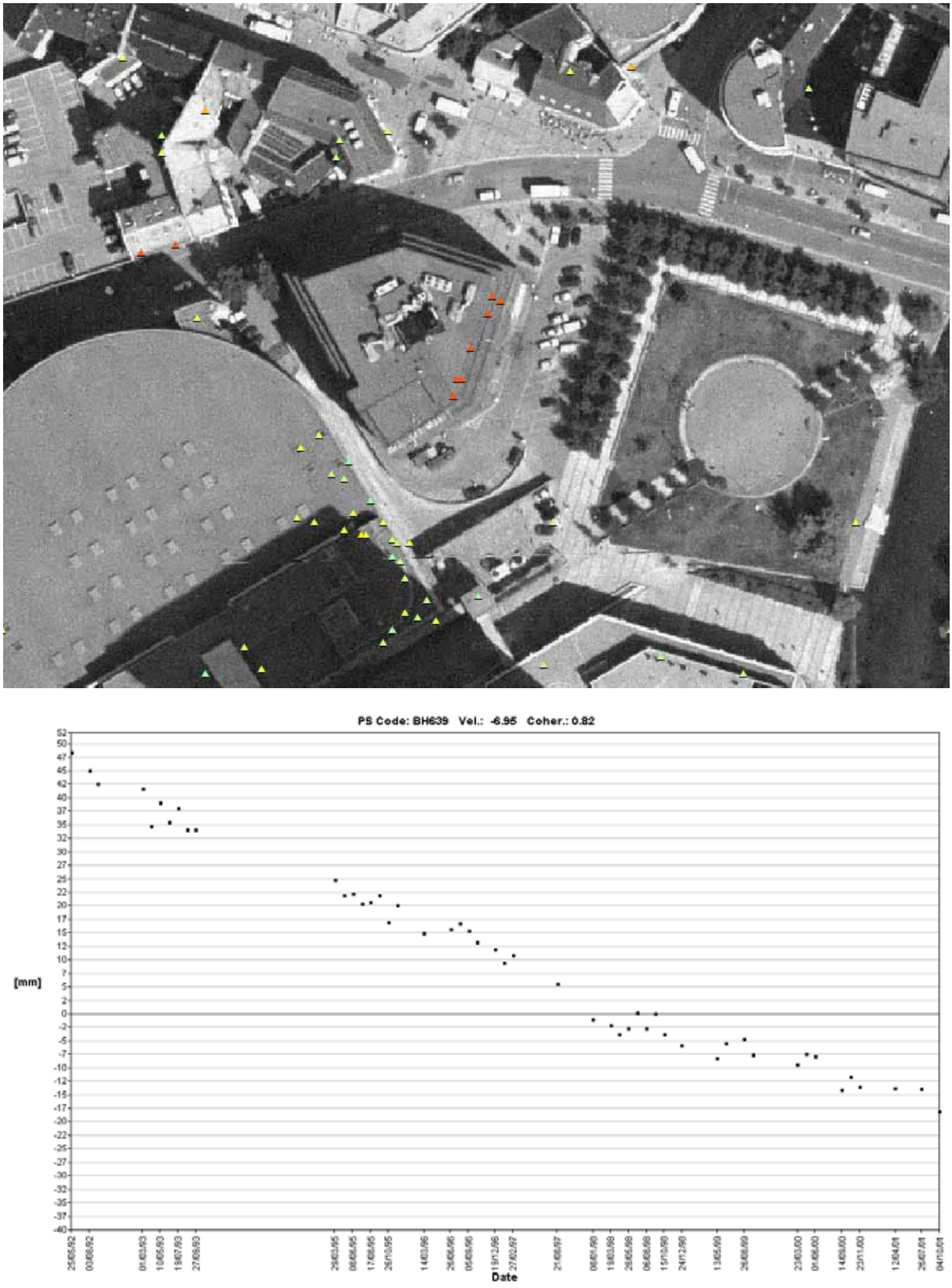

Figure 22. Displacement-time series from Lilletorget 1 (centre of photo).

3.6.5 Grev Wedels plass 1

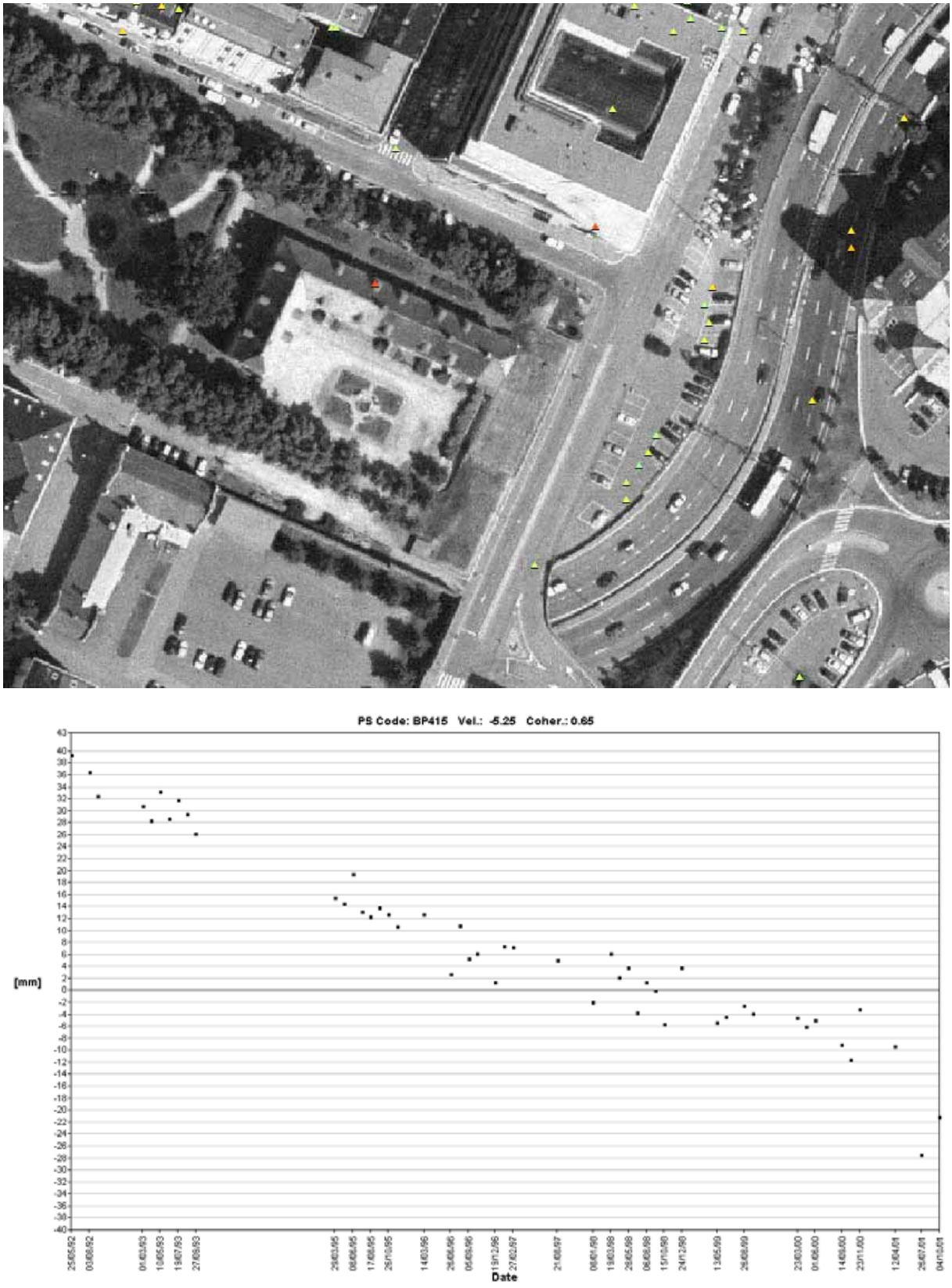

Figure 23. Displacement-time series from Grev Wedels plass 1 (centre of photo).

3.6.6 Rådhusplassen 1

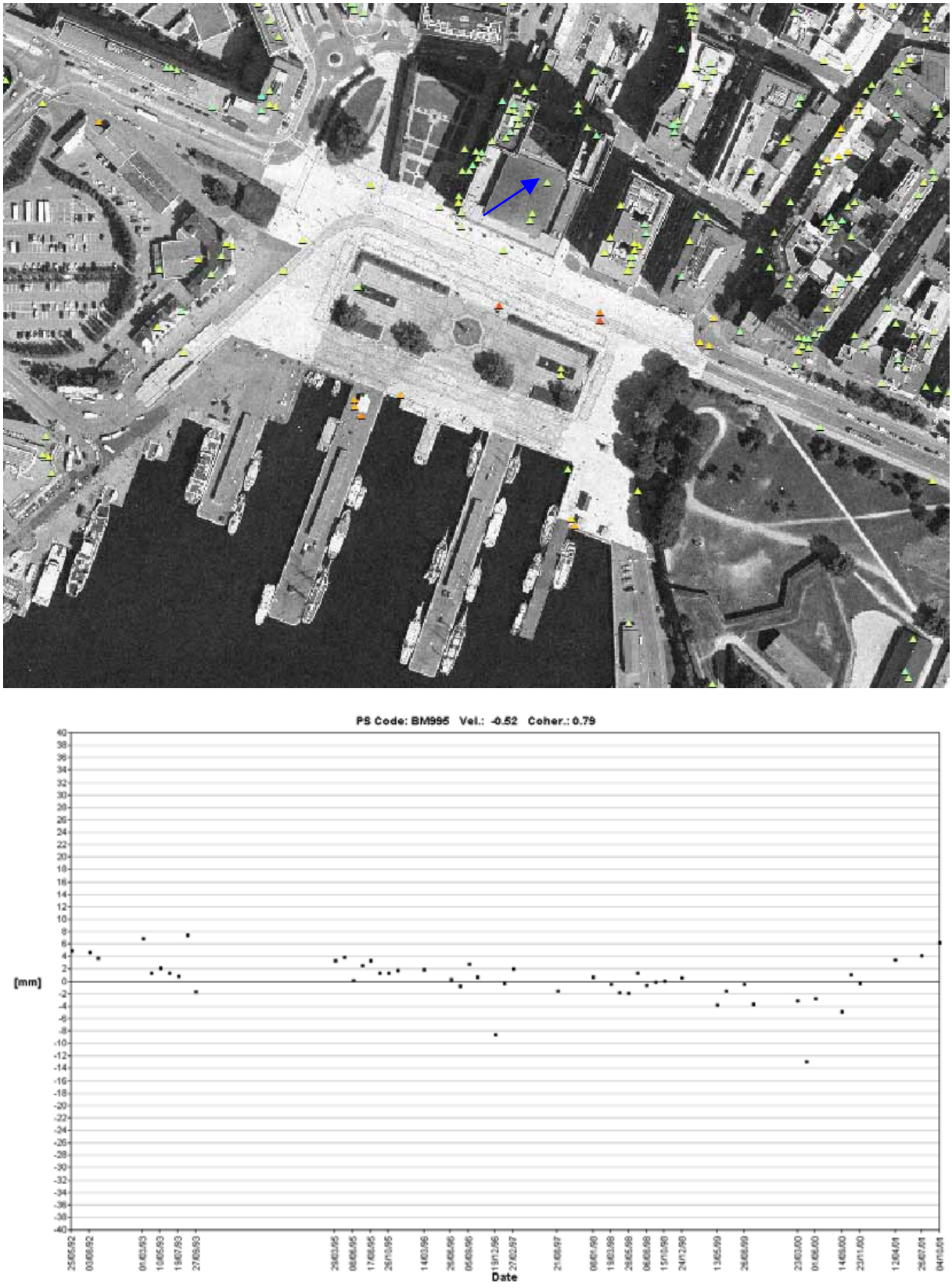

Figure 24. Displacement-time series from Rådhusplassen 1 (blue arrow).

3.6.7 Filipstad

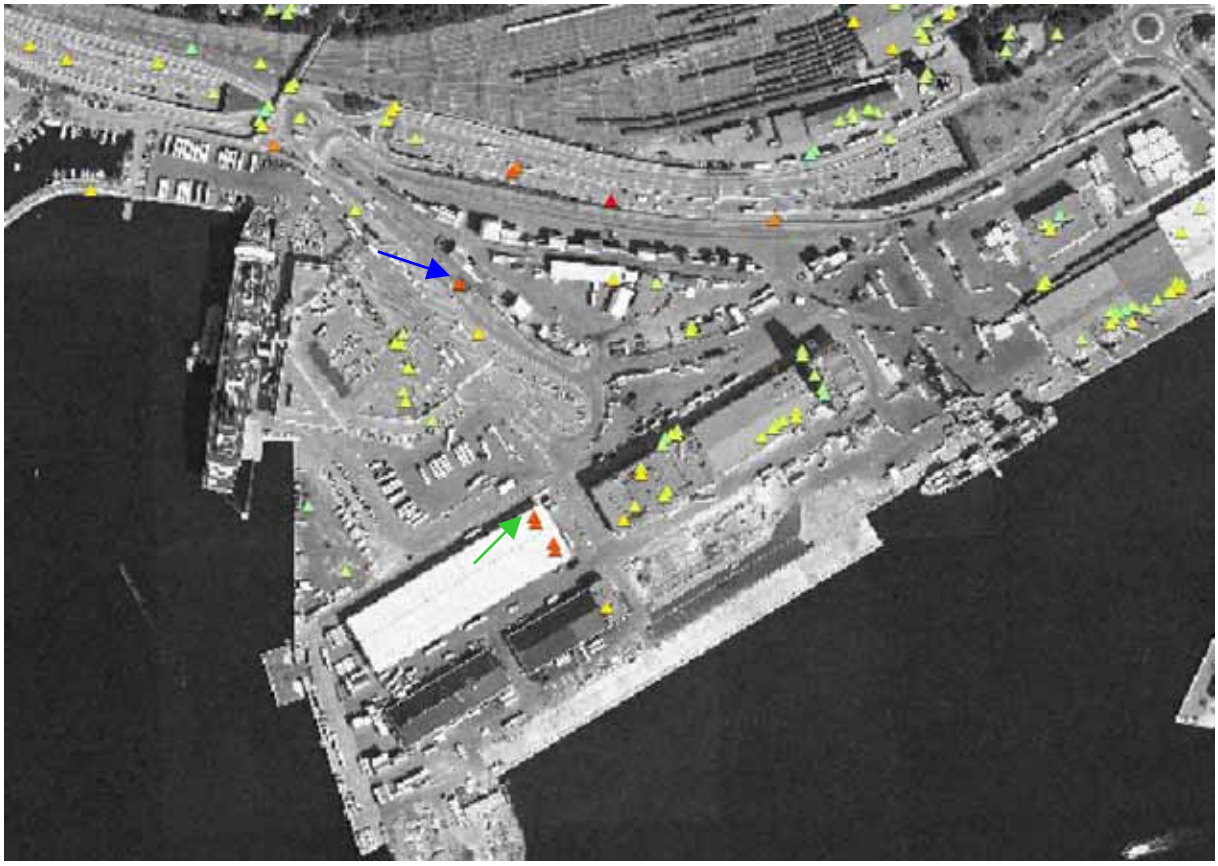

Figure 25. Subsidence pattern in Filipstad. Displacement-time series are shown in Figures 26 (blue arrow) and 27 (green arrow).

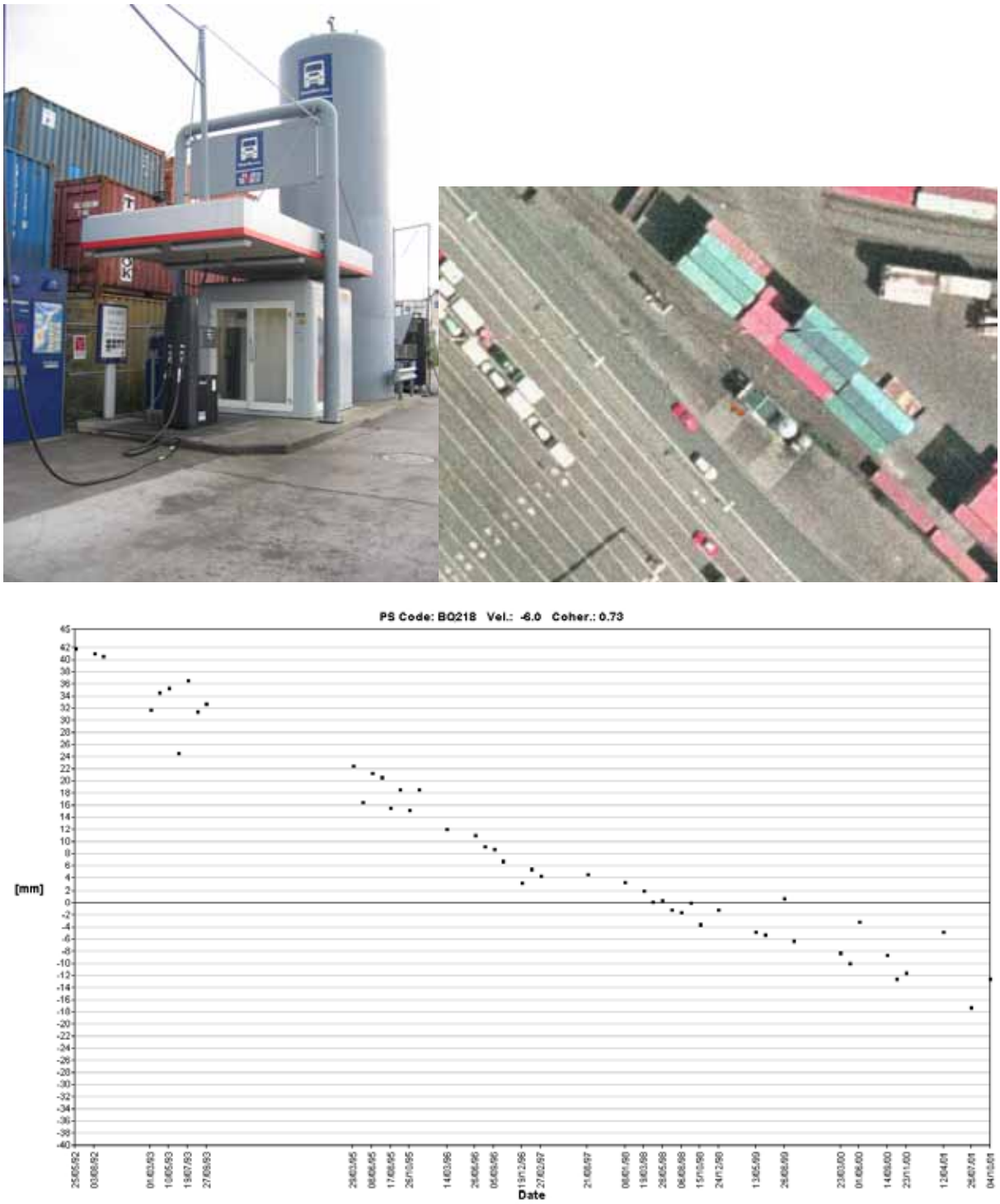

Figure 26. Displacement-time series from the gas station in Filipstad (see Figure 25 for location).

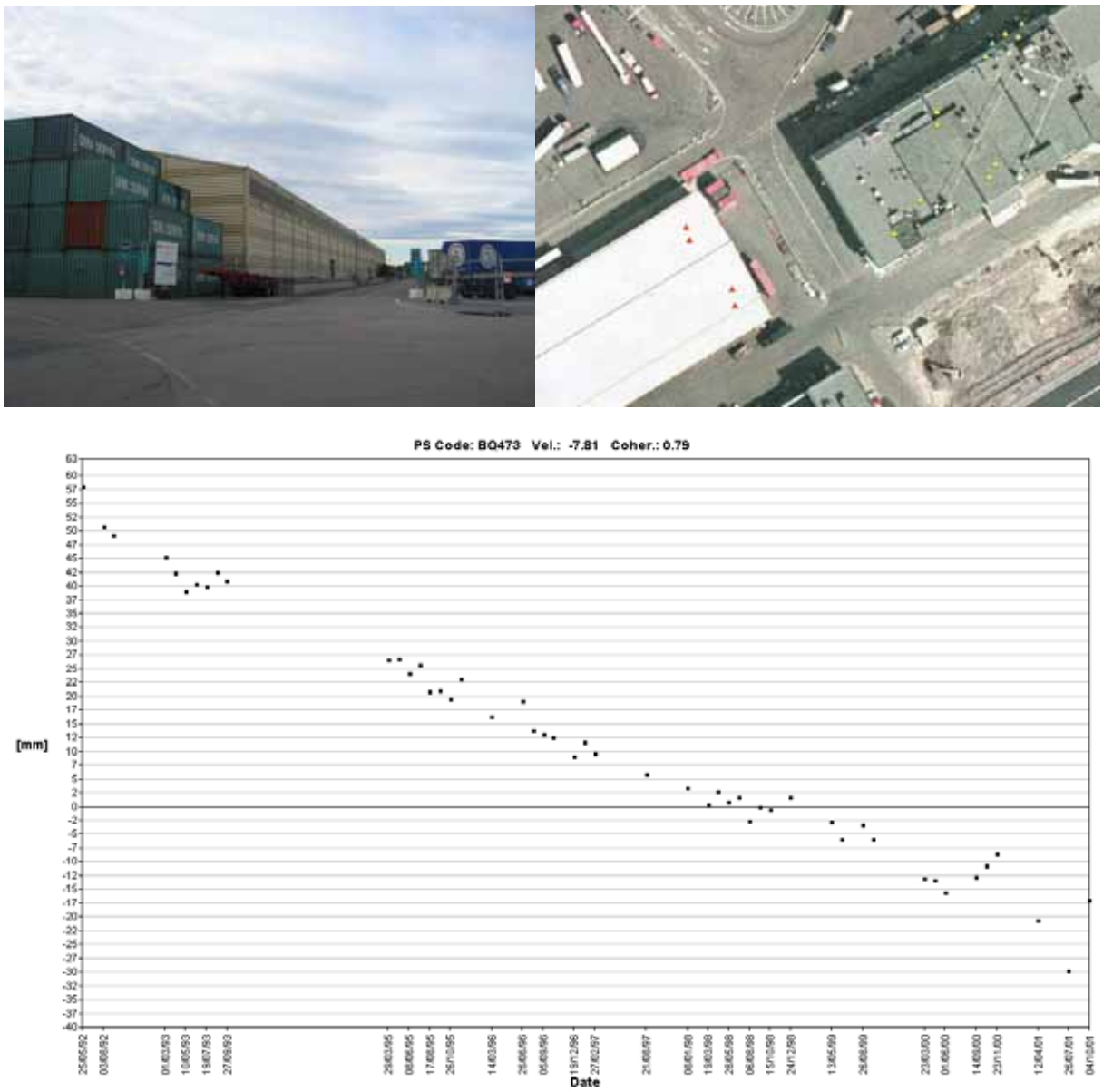

Figure 27. Displacement-time series from one of the warehouses in Filipstad (see Figure 25 for location).

3.6.8 Kongshavn kai/Sjursøya

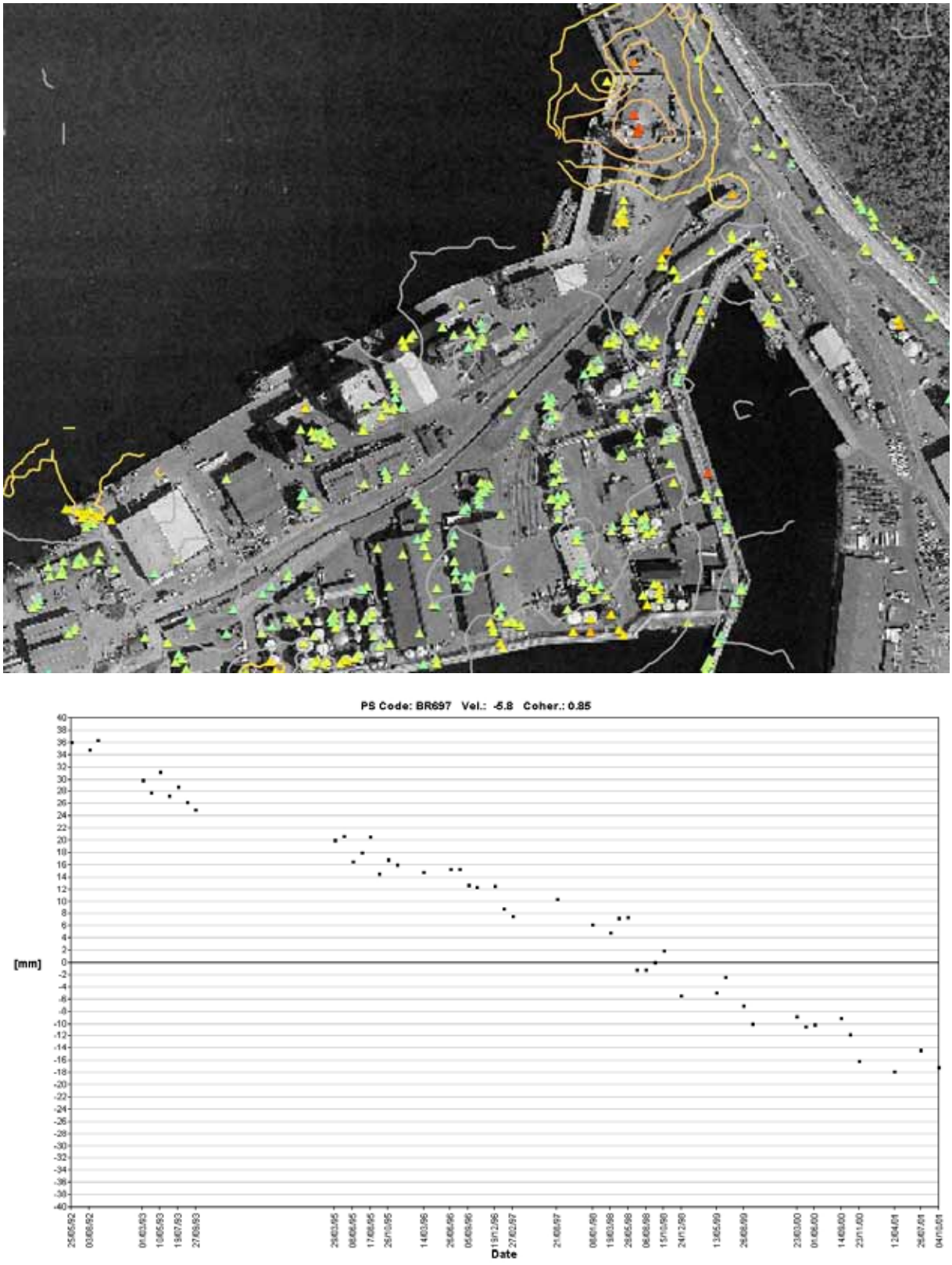

Figure 28. Displacement-time series from the northernmost building in Sjursøya.

3.6.9 Tøyen

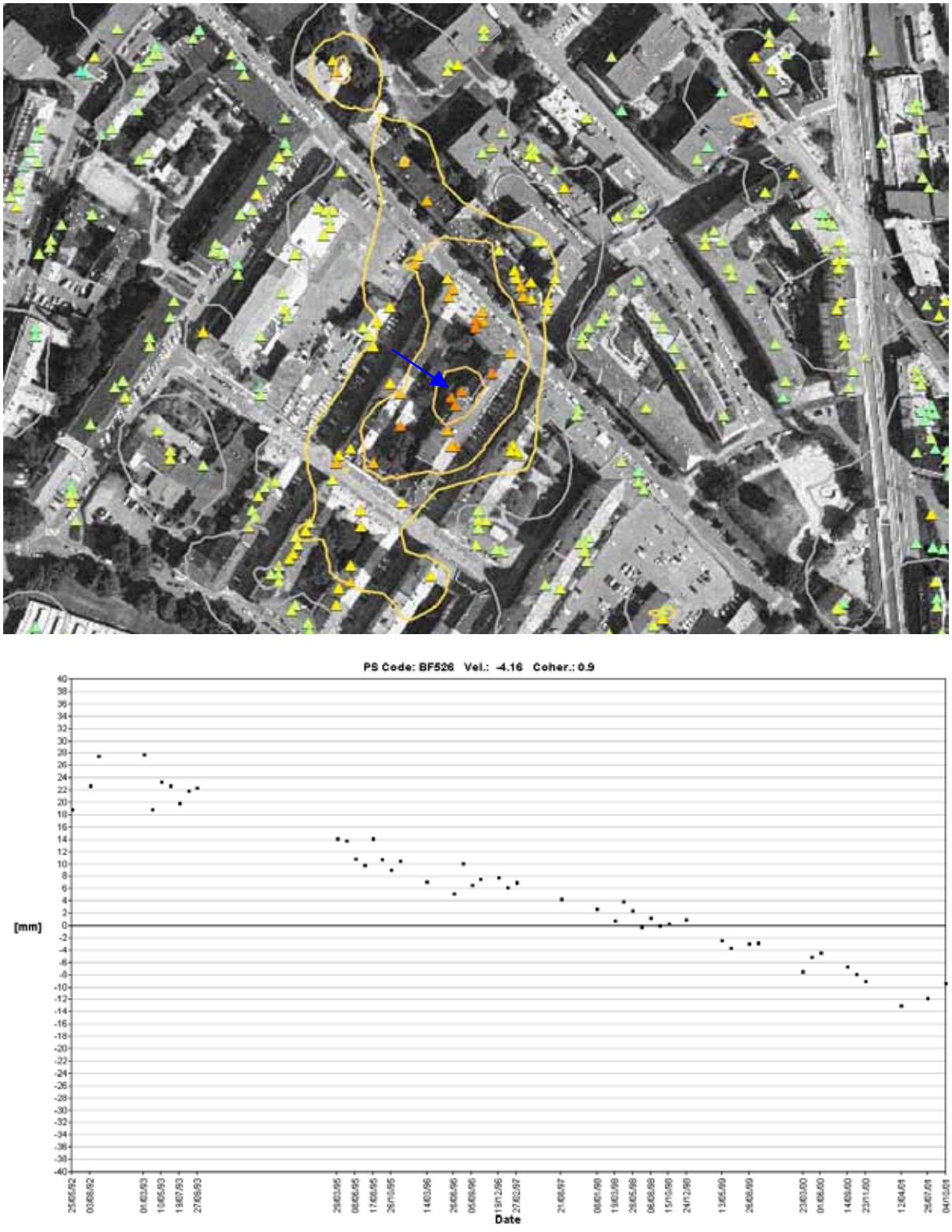

Figure 29. Displacement-time series from Eiriks Gata 17 (blue arrow).

3.6.10 Sofienberg

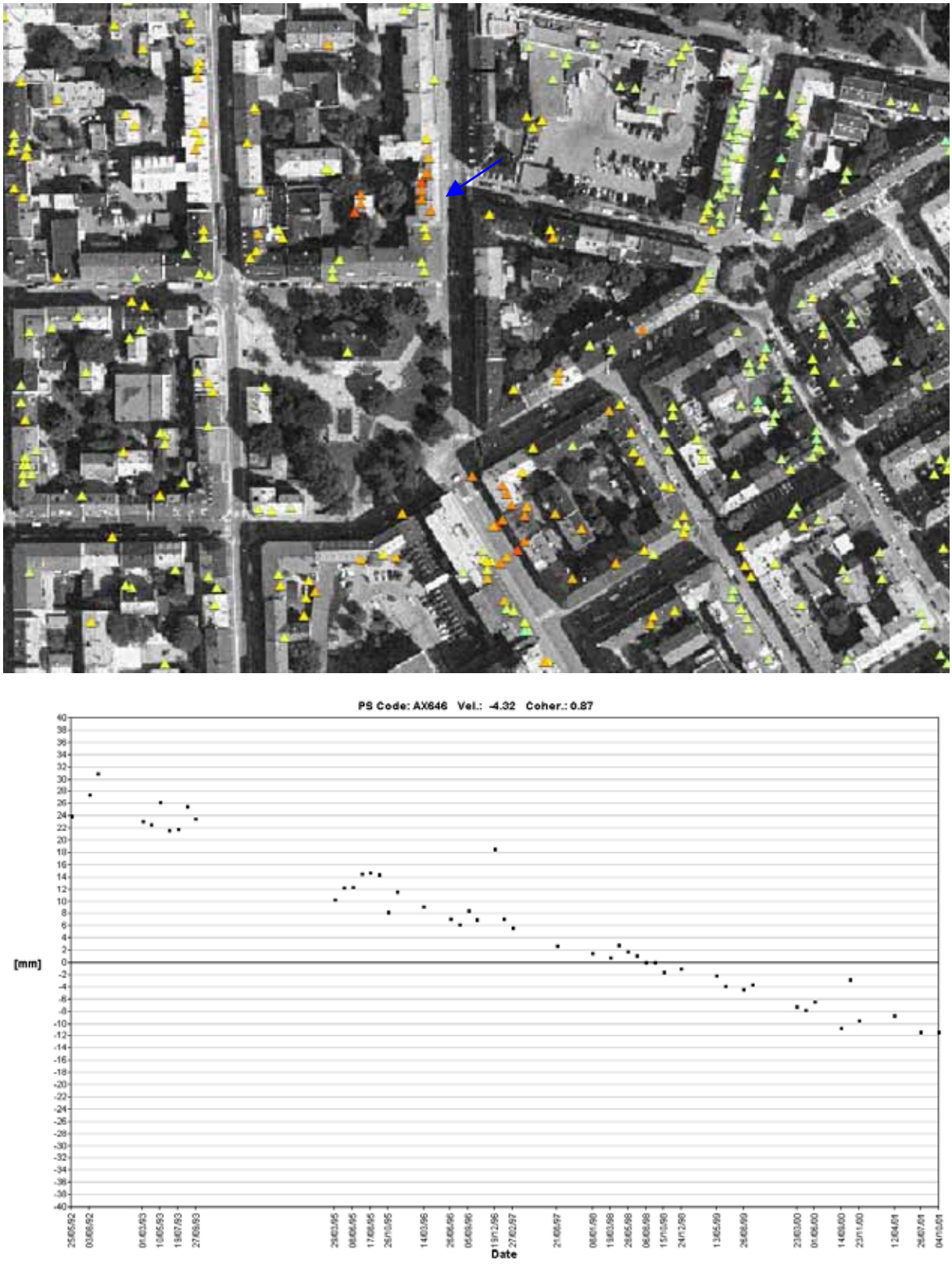

Figure 30. Displacement-time series from Toftes Gate 69 (blue arrow).

3.6.11 Ullevål

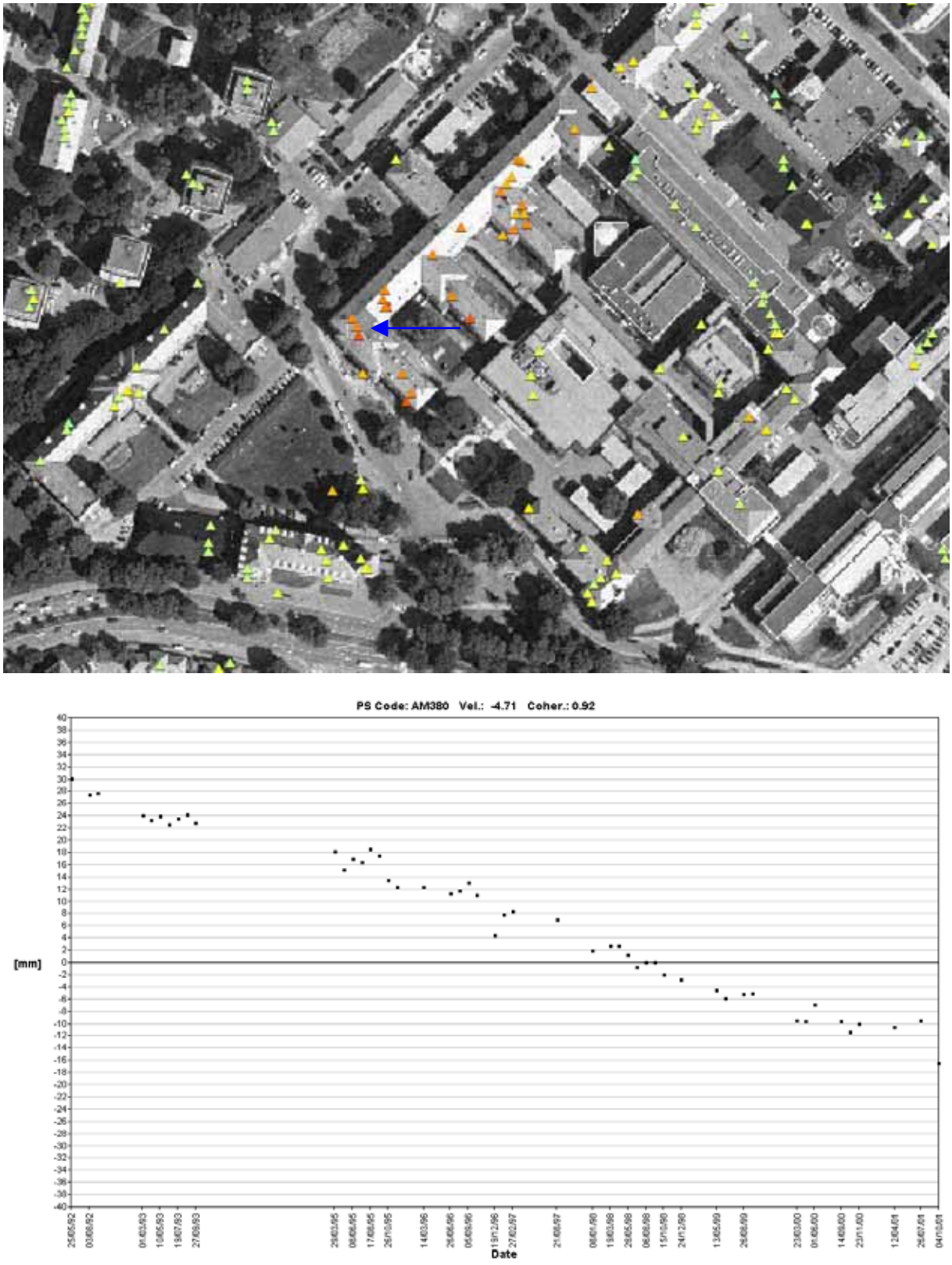

Figure 31. Displacement-time series from western corner of Ullevål hospital (blue arrow).

3.6.12 Majorstua

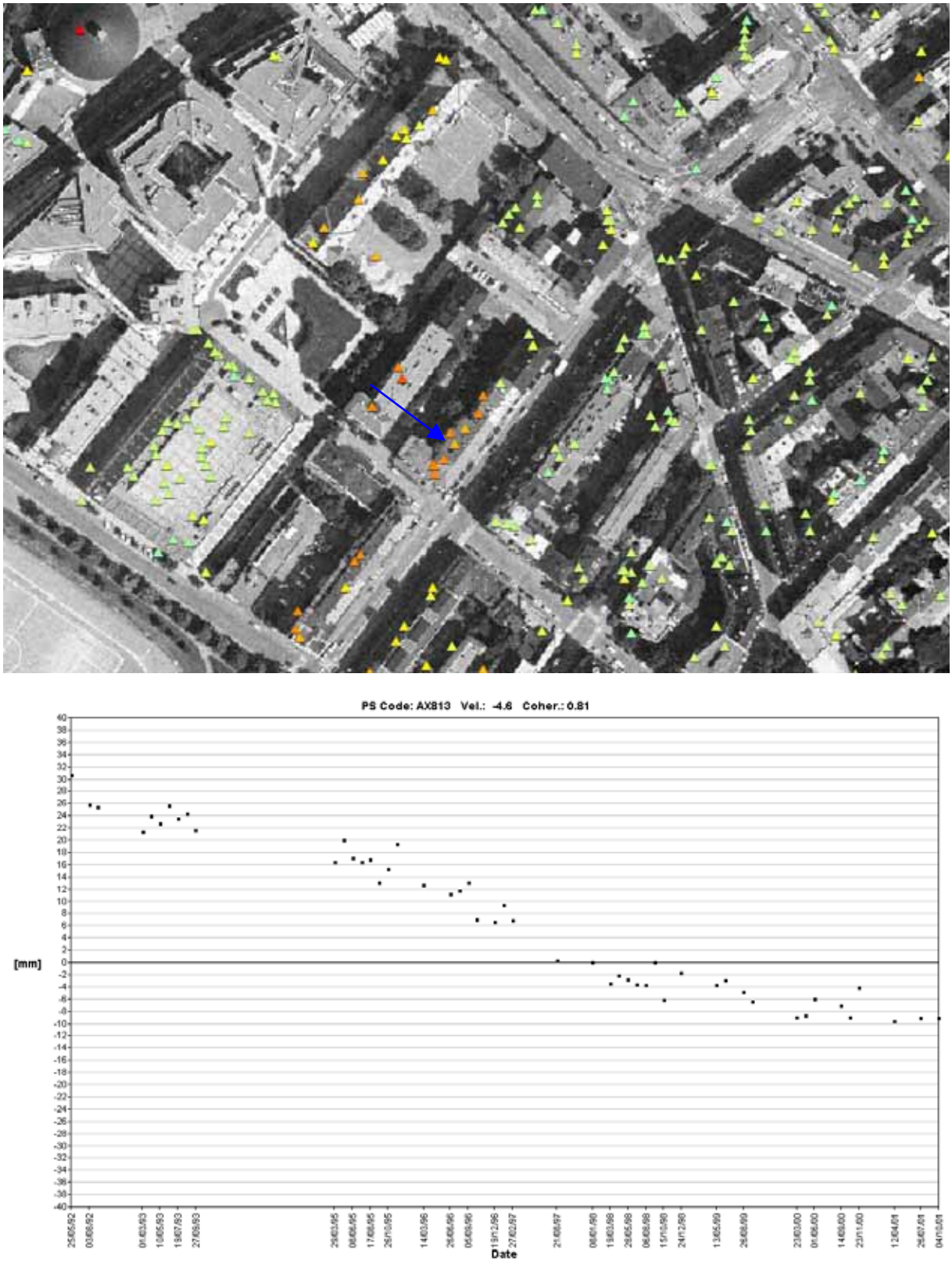

Figure 32. Displacement-time series from Kirkeveien 44 (blue arrow).

3.6.13 Colosseum Kino

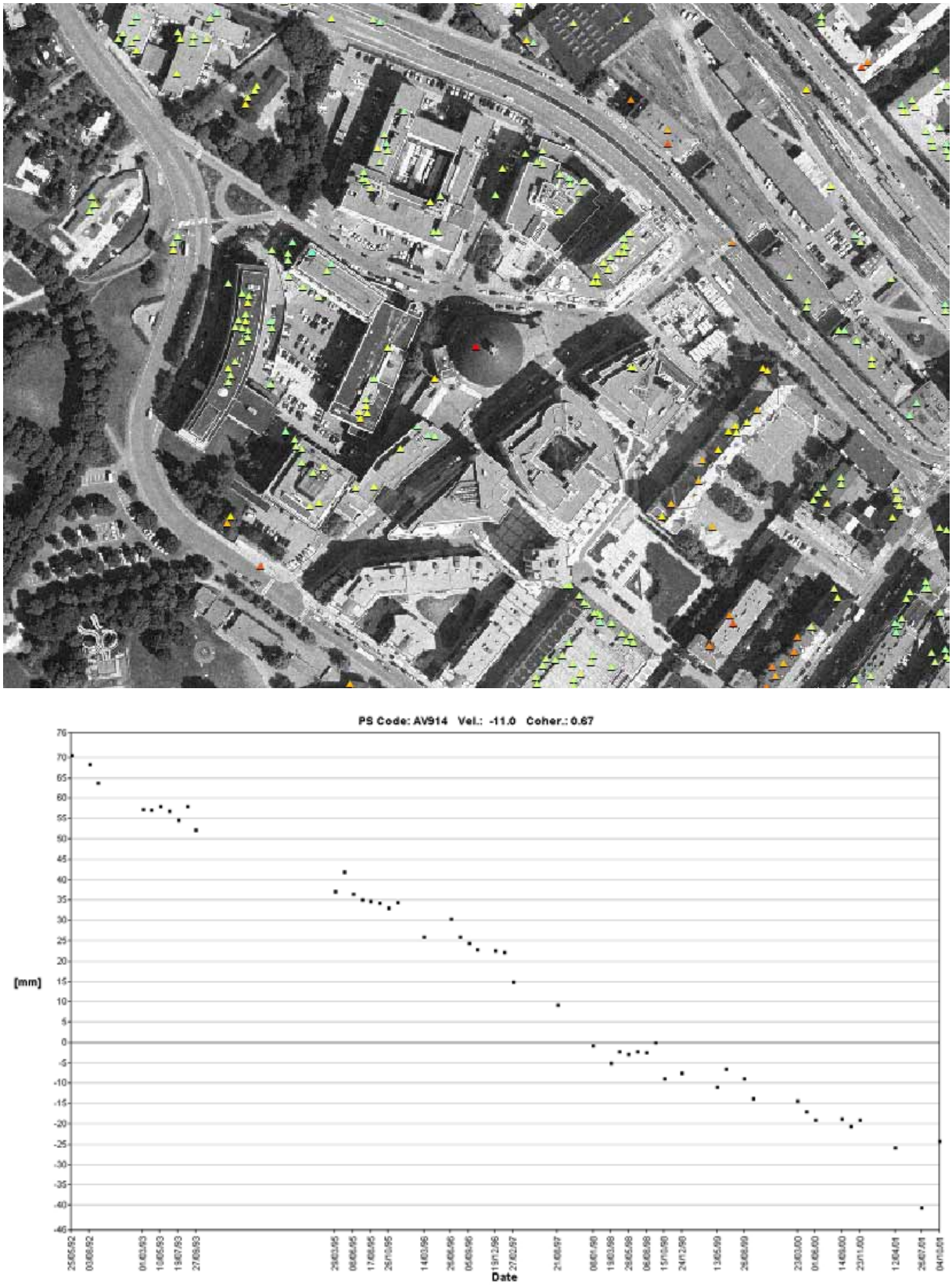

Figure 33. Displacement-time series from Fridtjof Nansensvei 8 (centre of photo).

3.6.14 Bislett stadion

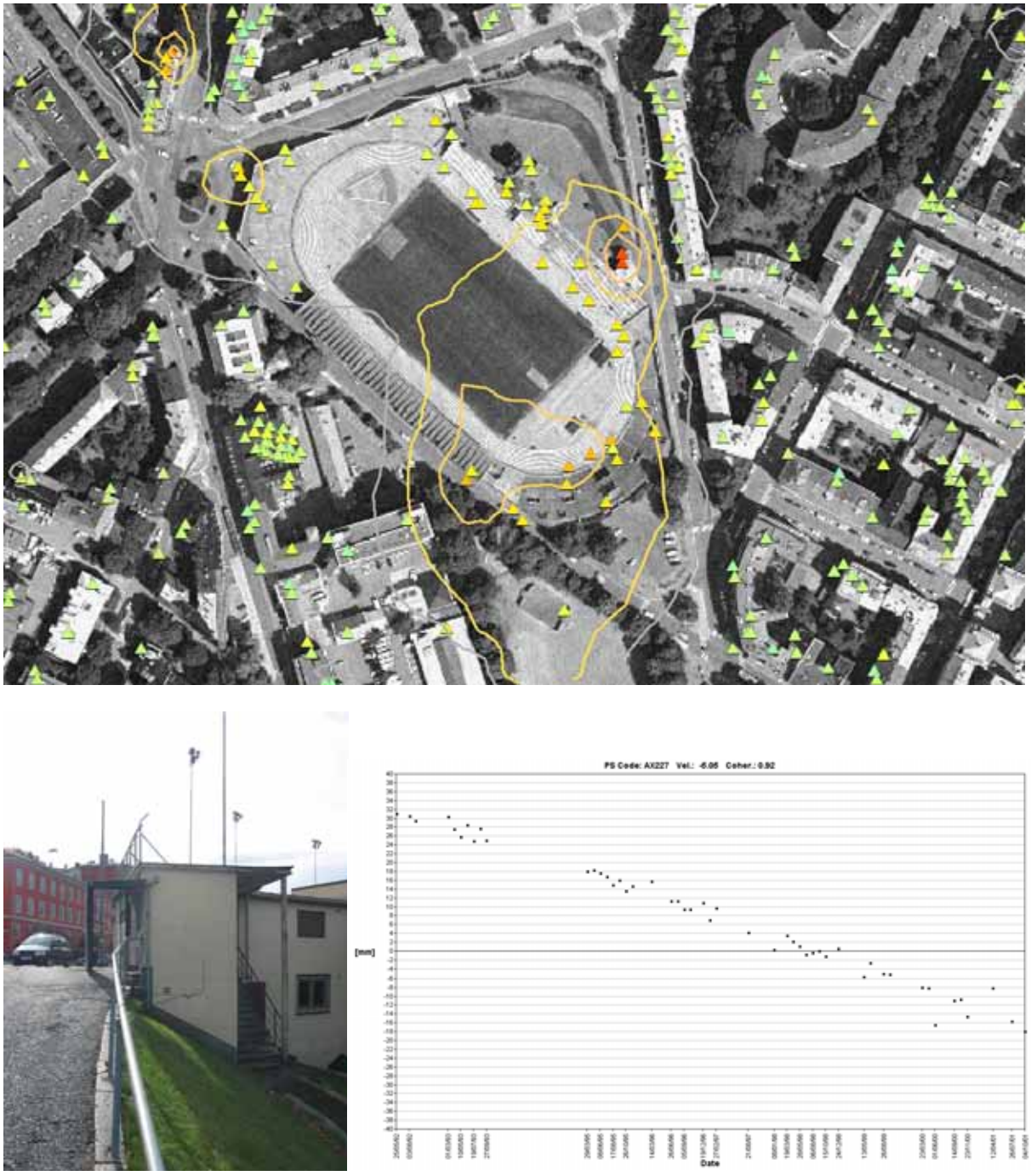

Figure 34. The area around Bislett stadium is subsiding between 1.5 and 2.0 mm/yr. Two PS have subsidence rate of 5 mm/yr, however these are located on the corner of a structure supported by a wooden post. It is most likely that this post is slowly deteriorating, leading to a slow collapse of the roof.

3.6.15 Frogner stadion

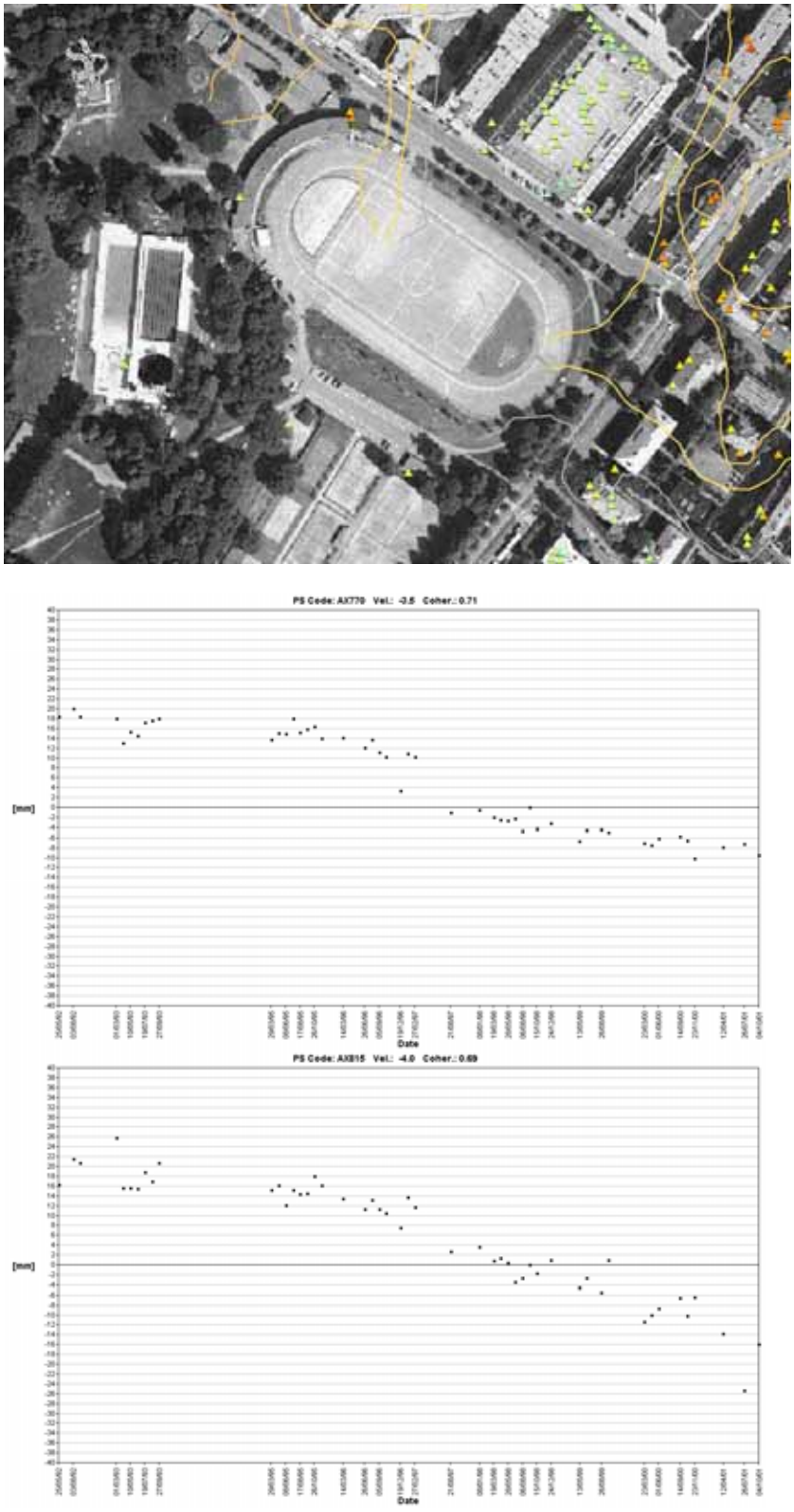

Figure 35. Only three PS were identified on Frogner stadion. According to the depth to bedrock map supplied by Oslo municipality, the stadium appears to be located on shallow sediments, with the exception of the northwestern and eastern corners. One of the PS identified is shows no subsidence. The other two are located on a structure on the northwestern corner of the stadium, and show subsidence rates of 3.5 to 4 mm/yr. No field checking has been carried out to determine if this represents true subsidence or slow collapse of the structure in question.

3.6.16 Jordal Amfi

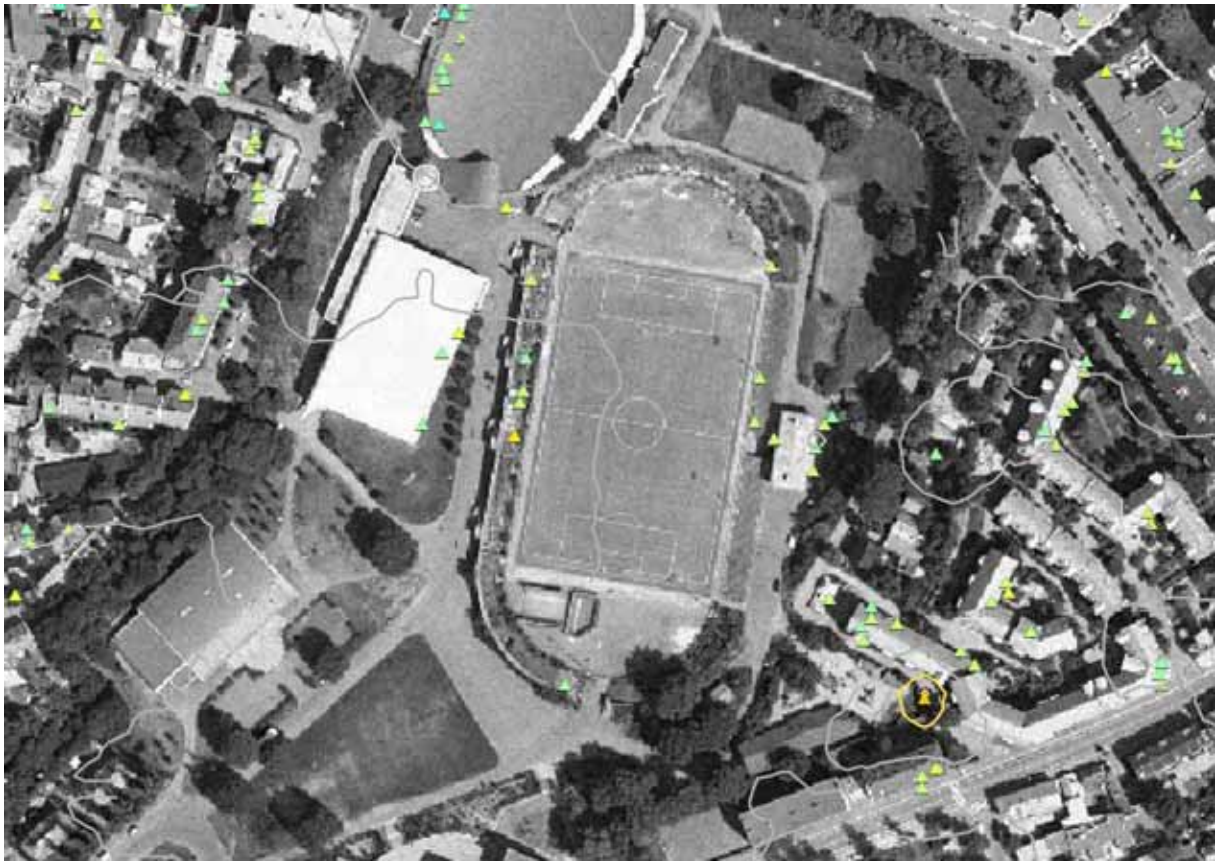

Figure 36. There is no evidence of subsidence in the area around Jordal Amfi.

3.6.17 Valle Hovin stadion

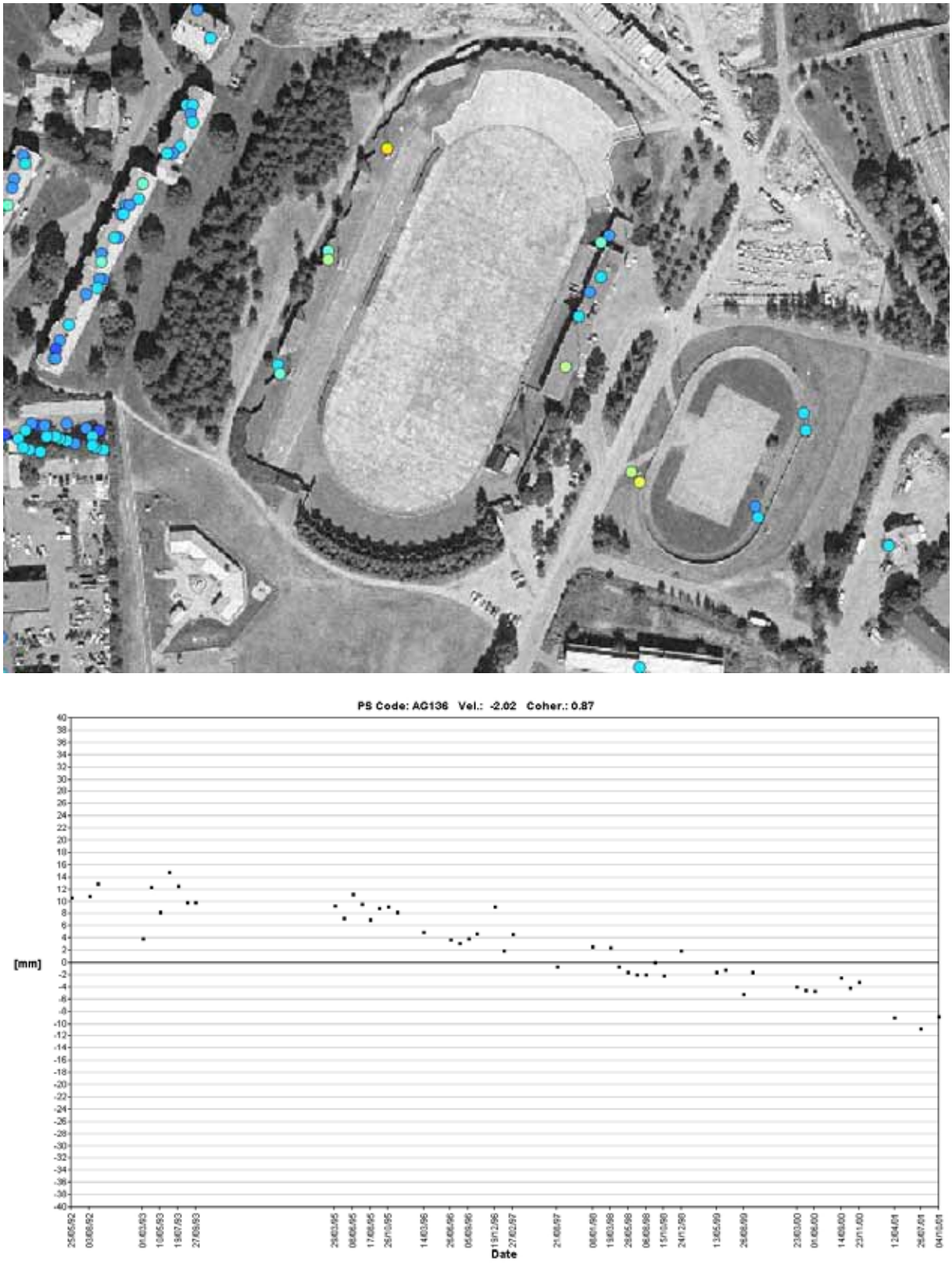

Figure 37. Only one point on Valle Hovin stadium shows any signs of subsidence (2 mm/yr). No visual inspection has been done.

4. FUTURE MONITORING POSSIBILITIES

The Permanent Scatters technique is based upon the availability of a time-series of SAR images. With the failure of gyroscope 1 onboard ERS-2 on January 7, 2001, very few images have been of sufficient quality to use for interferometry. The ESA satellite ENVISAT, launched in March, 2002, is in the same orbit as ERS-2 and able to obtain very similar images using it's ASAR instrument. It is possible to combine ERS and ASAR images to do PS analysis (ref). Unfortunately, the ASAR instrument currently only acquires images upon request. A 'background mission' has been asked for by a number of groups but it is still unclear how often the database of images will be updated. If we wish to study ongoing deformation, a new and more reliable source of images must be decided upon. The images for a given geographic area must be acquired using the same beam mode and geometry and must be acquired as regularly as possible. The Canadian Radarsat satellites offer the stability and reliability necessary to build up an archive of SAR images over Norway that can be used for current and future ground motion studies. Radarsat-1 was launched in November, 1995. Radarsat-2 is expected to be launched in 2006.

In January, 2003, the Norwegian Space Centre (Norsk Romsenter) signed an agreement with the Canadian Space Agency that assures access to Radarsat data to Norwegian public authorities. The agreement was based primarily on the need for scan-SAR images along the Norwegian coast to support ship detection and oil pollution applications. However, there is provision for the acquisition of a number of scan-SAR and standard mode scenes over the mainland. The main users of these data will be NVE (snow water equivalent determination) and NGU (ground motion detection and monitoring). Over the coming months, NGU will work together with Kongsberg Spacetec to plan image acquisition. It is hoped that we can begin acquiring scenes in early 2004 and have sufficient scenes by mid 2005 to begin monitoring critical areas. In the meantime, we will continue to use the ERS archive to identify areas at risk.

5. CONCLUSIONS

The Permanent Scatters technique has proven to be effective at identifying and quantifying subsidence over large areas with high accuracy and spatial resolution. PSInSAR measurements compared well with observations made with traditional surveying techniques. The average subsidence rate over a period of several years can be considered to be accurate to within 1 mm/yr. Individual displacement measurements within this period cannot be considered to be as accurate as those obtained by optical levelling. However, PSInSAR offers several advantages over traditional techniques. First, it is unique in being able to measure displacements at tens of thousands of points approximately every 35 days. Within central Oslo, over 20,000 PS were identified. In Hellerud and the surrounding region, over 10,000 were identified. Approximately one third of these have a high enough signal-to-noise ratio to construct displacement-time series. Secondly, it is the only technique available that allows us to identify and measure displacements that took place years ago by taking advantage of the European Space Agency's archive.

In this report we do not try to draw any conclusions regarding the causes of subsidence. Proper understanding of the pattern of subsidence would require access to other data, including surficial sediment type and thickness, groundwater information, locations of anthropogenic fill and excavation activities. It is hoped that the highly detailed picture of subsidence obtained by this study can be used in the future to better understand the details of the processes involved and predict and prevent future problems.

We intend to begin the process of building an archive of new SAR images over several cities in Norway, as well as areas of higher than average landslide risk. We are also cooperating with other Geological Surveys across Europe to establish a ground-motion monitoring service supported by both governmental and commercial users.

6. REFERENCES

Amelung, F., Galloway, D., Bell, J., Zebker, H., and Laczniak, R., 1999, Sensing the ups and downs of Las Vegas: InSAR reveals structural control of land subsidence and aquifer-system deformation: Geology, v. 27, p. 483-486.

Colesanti, C., Ferretti, A., Novali, F., Prati, C., and Rocca, F., 2003a, SAR monitoring of progressive and seasonal ground deformation using the Permanent Scatterers Technique: IEEE Transactions on Geoscience and Remote Sensing, v. 41, p. 1685-1701.

Colesanti, C., Ferretti, A., Prati, C., and Rocca, F., 2003b, Monitoring landslides and tectonic motions with the Permanent Scatterers Technique: Engineering Geology, v. 68, p. 3-14.

Dehls, J.F., Basilico, M., and Colesanti, C., 2002, Ground deformation monitoring in the Ranafjord area of Norway by means of the Permanent Scatterers technique, Geoscience and Remote Sensing Symposium, 2002. IGARSS '02. 2002 IEEE International, Volume 1: Toronto, p. 203-207.

Faggruppen for setningsskader, 2002, Romeriksporten - setningsskader, Vurdering av skader og tiltak: Oslo, p. 10.

Ferretti, A., Prati, C., and Rocca, F., 2001, Permanent scatterers in SAR interferometry: IEEE Transactions on Geoscience and Remote Sensing, v. 39, p. 8-20.

Fruneau, B., and Sarti, F., 2000, Detection of ground subsidence in the city of Paris using radar interferometry: isolation of deformation from atmospheric artifacts using correlation: Geophysical Research Letters, v. 27, p. 3981-3984.

Galloway, D., Hudnut, K., Ingebritsen, S., Phillips, S., Peltzer, G., Rogez, F., and Rosen, P., 1998, Detection of aquifer system compaction and land subsidence using interferometric synthetic aperture radar, Antelope Valley, Mojave Desert, California: Water Resources Research, v. 34, p. 2573-2585.

Massonnett, D., Rossi, M., Carmona, C., Adragna, F., Peltzer, G., Feigl, K., and Rabaute, T., 1993, The displacement field of the Landers earthquake mapped by radar interferometry: Nature, v. 364, p. 138-142.

Rosenbaum, M.S., and Culshaw, M.G., 2003, Communicating the risks arising from geohazards: Journal of the Royal Statistical Society, Series A, v. 166, p. 261-270.

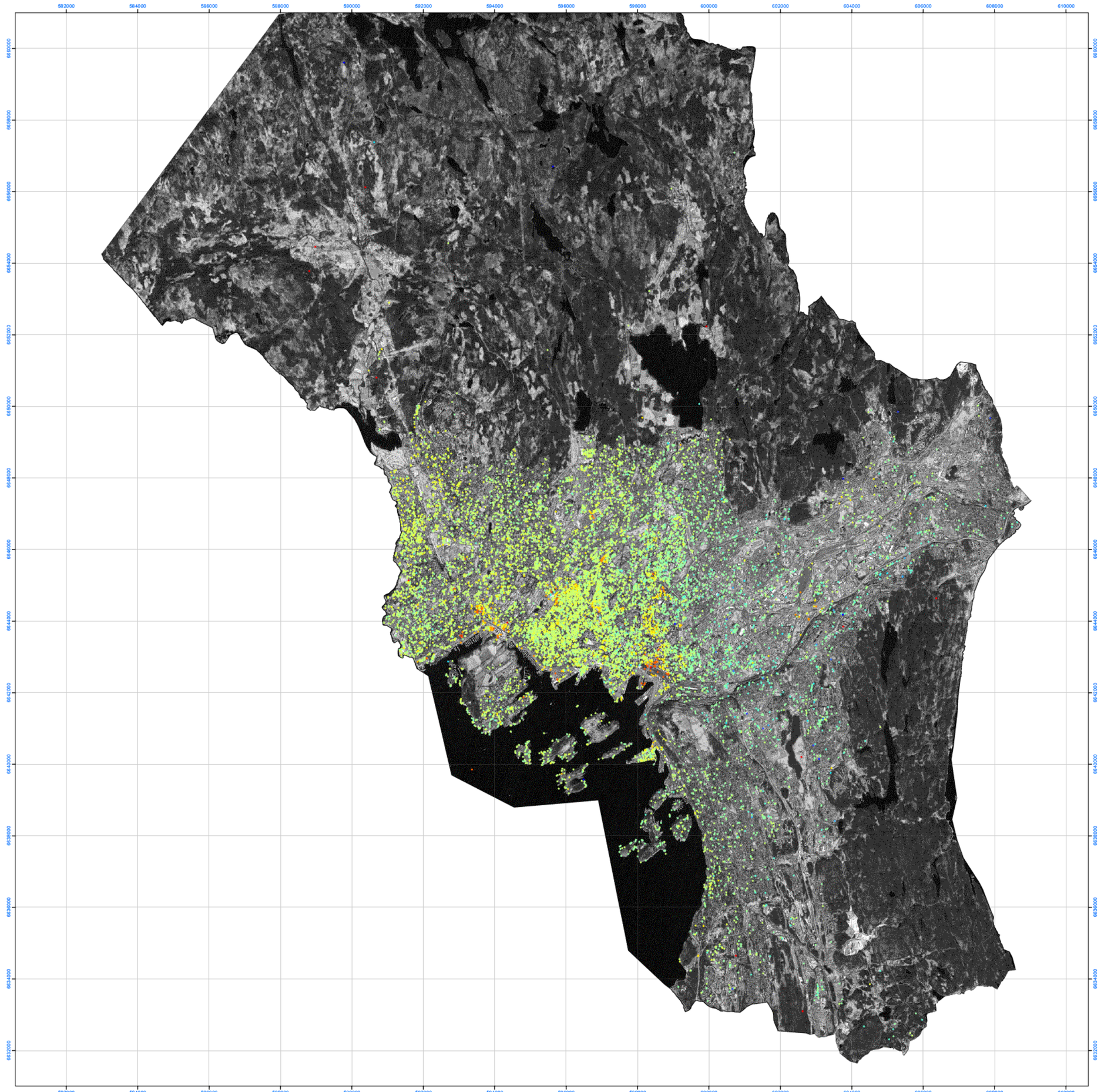

NGU
Norges geologiske undersøkelse
Geological Survey of Norway

Track 108, Frame 2394

mm/yr

- -27,00 - -9,00
- -8,99 - -5,00
- -4,99 - -4,00
- -3,99 - -3,00
- -2,99 - -2,00
- -1,99 - -1,00
- -0,99 - 0,00
- 0,01 - 1,00
- 1,01 - 2,00
- 2,01 - 3,00
- 3,01 - 4,00
- 4,01 - 5,00
- 5,01 - 9,00
- 9,01 - 30,00

AVERAGE RELATIVE VELOCITY, 1993-2002, FROM DIFFERENTIAL RADAR INTERFEROMETRY

ERS Track 108, Frame 2394
Oslo

Drawing: Dehls, J. F.	**Date:** DEC 2003	
Scale 1:50 000 1,000 500 0 1,000 2,000 3,000 4,000 metres		**Mapsheet (1:50 000):** 1814 I Asker 1914 IV Oslo
NGU Geology for Society since 1858	**GEOLOGICAL SURVEY OF NORWAY** Leiv Eirikssons vei 39 NO-7491 TRONDHEIM Tel +47-73 90 40 00, Fax +47-73 92 16 20 http://www.ngu.no	**Drawing no:** **2003.105-01**

TRE TELE-RILEVAMENTO EUROPA
a POLIMI spin-off company

PSInSAR processing performed by
Tele-Rilevamento Europa - T.R.E. s.r.l.
http://www.treuropa.com

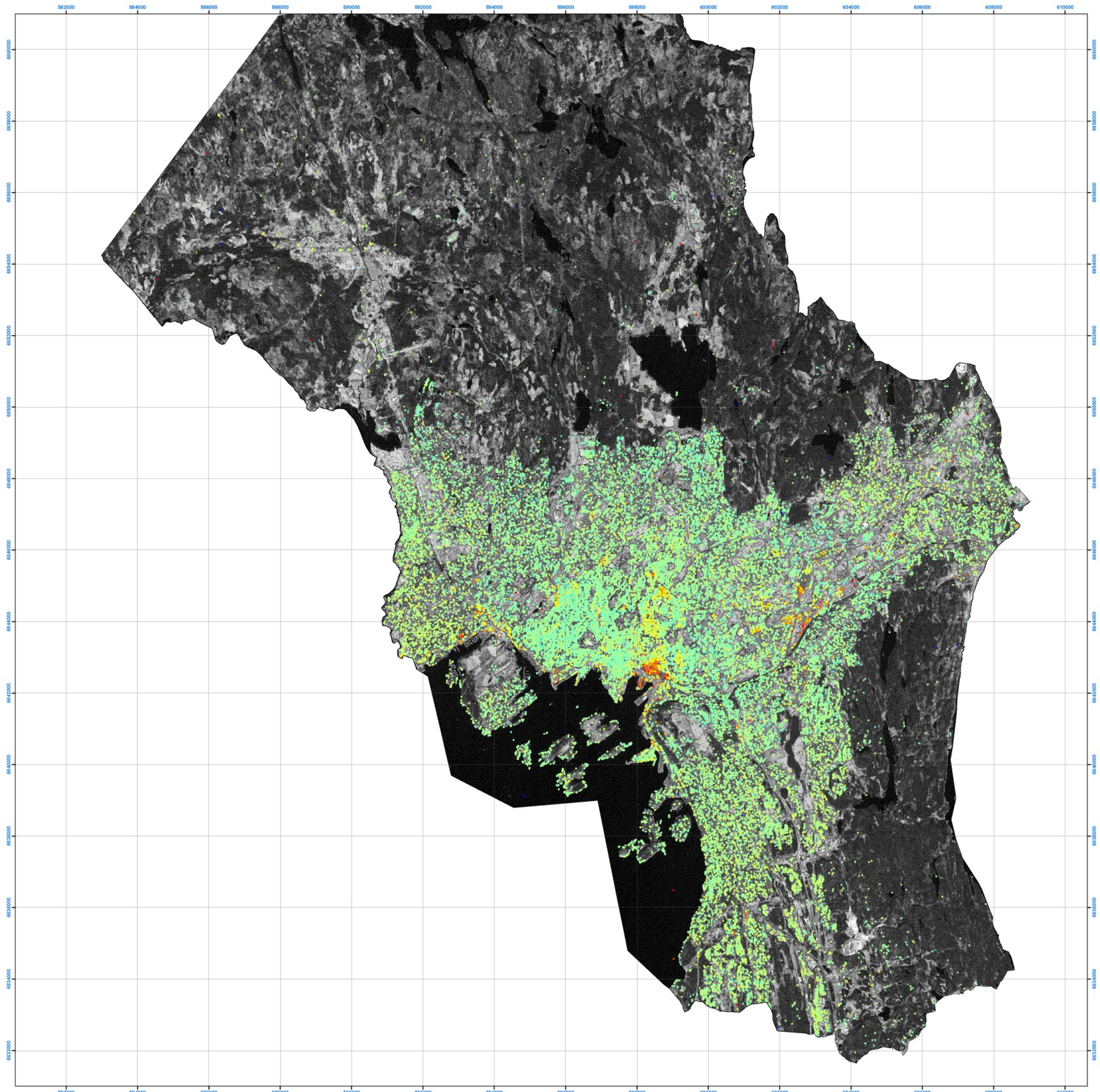

NGU
Norges geologiske undersøkelse
Geological Survey of Norway

Track 337, Frame 2396

Vel

- -27,00 - -9,00
- -8,99 - -5,00
- -4,99 - -4,00
- -3,99 - -3,00
- -2,99 - -2,00
- -1,99 - -1,00
- -0,99 - 0,00
- 0,01 - 1,00
- 1,01 - 2,00
- 2,01 - 3,00
- 3,01 - 4,00
- 4,01 - 5,00
- 5,01 - 9,00
- 9,01 - 30,00

AVERAGE RELATIVE VELOCITY, 1992-2001, FROM DIFFERENTIAL RADAR INTERFEROMETRY

ERS Track 337, Frame 2396
Oslo

Drawing: Dehls, J. F. | **Date:** DEC 2003

Scale 1:50 000

1,000 500 0 1,000 2,000 3,000 4,000
metres

Mapsheet (1:50 000):
1814 I Asker
1914 IV Oslo

NGU
Geology for Society since 1858

GEOLOGICAL SURVEY OF NORWAY
Leiv Eirikssons vei 39
NO-7491 TRONDHEIM
Tel +47-73 90 40 00, Fax +47-73 92 16 20
http://www.ngu.no

Drawing no:
2003.105-02

TRE TELE-RILEVAMENTO EUROPA
a POLIMI spin-off company

PSInSAR processing performed by
Tele-Rilevamento Europa - T.R.E. s.r.l.
http://www.treuropa.com

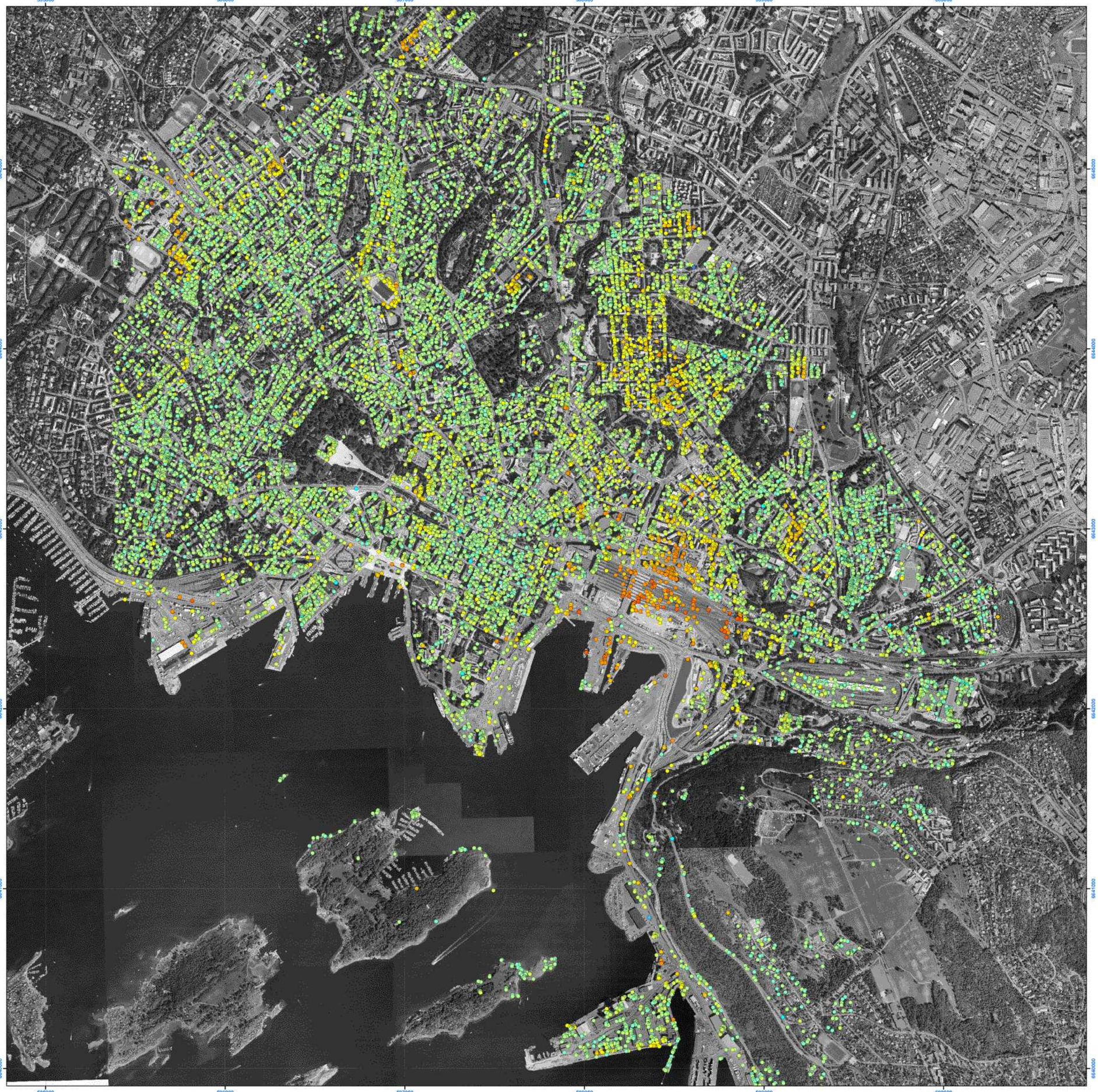

NGU
Norges geologiske undersøkelse
Geological Survey of Norway

Vel
-23.00
-22.99 - -9.00
-8.99 - -5.00
-4.99 - -3.00
-2.99 - -2.00
-1.99 - -1.00
-0.99 - 0.00
0.01 - 1.00
1.01 - 2.00
2.01 - 4.00
4.01 - 5.00
5.01 - 9.00
9.01 - 15.00

AVERAGE RELATIVE VELOCITY, 1992-2001, FROM DIFFERENTIAL RADAR INTERFEROMETRY

ERS Track 337, Frame 2396
Oslo (Centre, Majorstua, Ullevål, Sjursøya)

Drawing: Dehls, J. F.	Date: DEC 2003	
Scale 1:10 000 200 100 0 200 400 600 800 metres		Mapsheet (1:50 000): 1814 I Asker 1914 IV Oslo
NGU Geology for Society since 1858	GEOLOGICAL SURVEY OF NORWAY Leiv Eirikssons vei 39 NO-7491 TRONDHEIM Tel +47-73 90 40 00, Fax +47-73 92 16 20 http://www.ngu.no	Drawing no: 2003.105-03

TRE TELE-RILEVAMENTO EUROPA

PSInSAR processing performed by
Tele-Rilevamento Europa - T.R.E. s.r.l.
http://www.treuropa.com

601000 602000 603000 604000 605000 606000

6644000 6643000 6642000 6641000

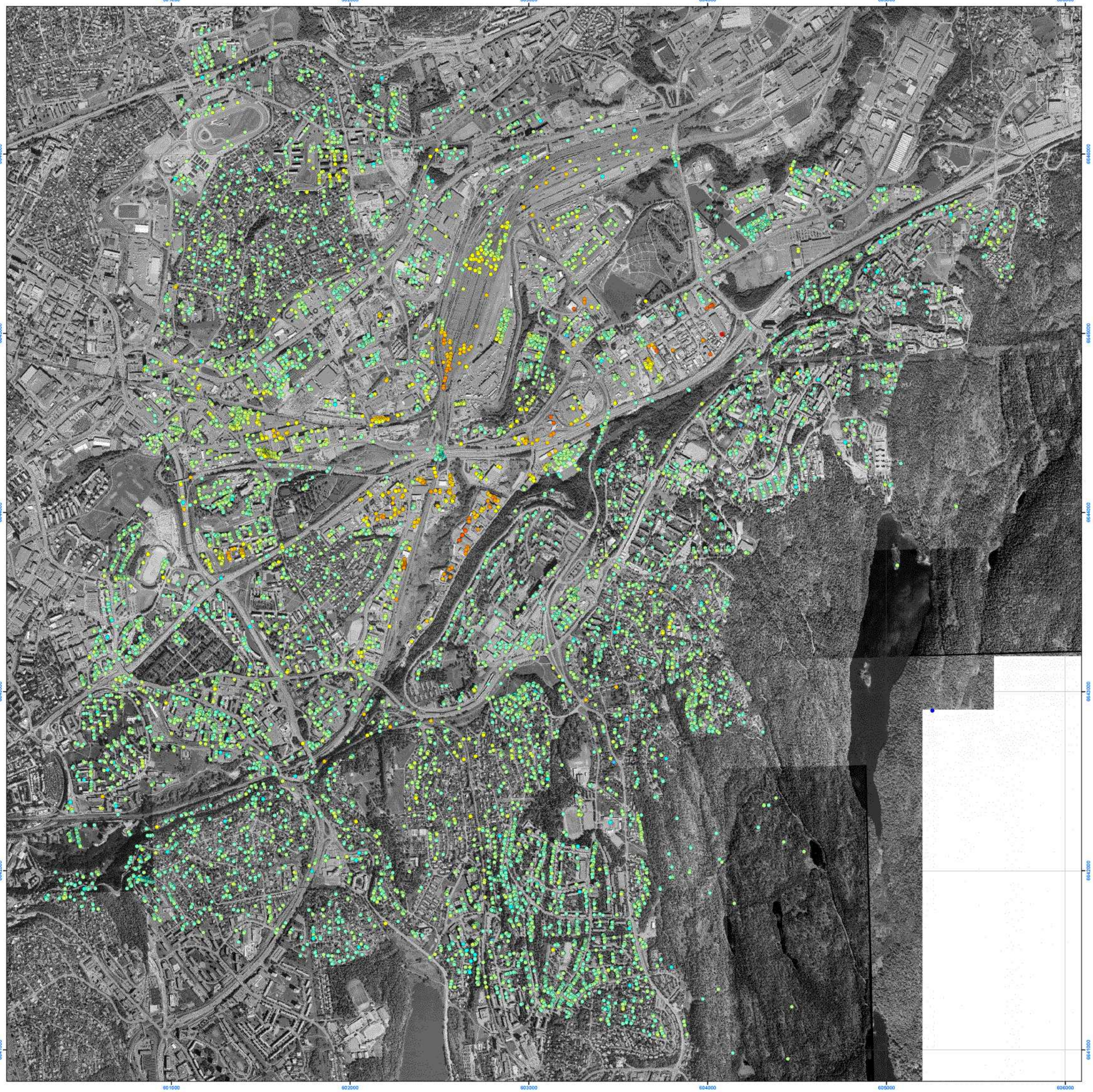

NGU
Norges geologiske undersøkelse
Geological Survey of Norway

1992-2001 (mm/yr)

- -23.00
- -22.99 - -9.00
- -8.99 - -5.00
- -4.99 - -3.00
- -2.99 - -2.00
- -1.99 - -1.00
- -0.99 - 0.00
- 0.01 - 1.00
- 1.01 - 2.00
- 2.01 - 4.00
- 4.01 - 5.00
- 5.01 - 9.00
- 9.01 - 15.00

AVERAGE RELATIVE VELOCITY, 1992-2001, FROM DIFFERENTIAL RADAR INTERFEROMETRY

ERS Track 337, Frame 2396
Oslo (Helsfyr, Alna, Lutvann)

Drawing: Dehls, J. F.	**Date:** DEC 2003	
Scale 1:10 000 200 100 0 200 400 600 800 metres		**Mapsheet (1:50 000):** 1914 IV Oslo
NGU Geology for Society since 1858 **GEOLOGICAL SURVEY OF NORWAY** Leiv Eirikssons vei 39 NO-7491 TRONDHEIM Tel +47-73 90 40 00, Fax +47-73 92 16 20 http://www.ngu.no		**Drawing no:** **2003.105-04**

PSInSAR processing performed by
Tele-Rilevamento Europa - T.R.E. s.r.l.
http://www.treuropa.com